ORIGINAL ARTICLE

Ramisyllis kingghidorahi n. sp., a new branching annelid from Japan

M. Teresa Aguado[1] · **Guillermo Ponz-Segrelles[2]** · **Christopher J. Glasby[3]** · **Rannyele P. Ribeiro[4,5]** · **Mayuko Nakamura[6]** · **Kohei Oguchi[6,7]** · **Akihito Omori[8]** · **Hisanori Kohtsuka[6]** · **Christian Fisher[1]** · **Yuji Ise[9]** · **Naoto Jimi[10]** · **Toru Miura[6]**

Abstract

Among over 20,000 species of Annelida, only two branching species with a highly modified body-pattern are known until now: the Syllidae *Syllis ramosa* McIntosh, 1879, and *Ramisyllis multicaudata* Glasby et al. (Zoological Journal of the Linnean Society, 164, 481–497, 2012). Both have unusual ramified bodies with one head and multiple branches and live inside the canals of host sponges. Using an integrative approach (combining morphology, internal anatomy, ecology, phylogeny, genetic divergence, and the complete mitochondrial genome), we describe a new branching species from Japan, *Ramisyllis kingghidorahi* n. sp., inhabiting an undescribed species of *Petrosia* (Porifera: Demospongiae) from shallow waters. We compare the new species with its closest relative, *R. multicaudata*; emend the diagnosis of *Ramisyllis*; and discuss previous reports of *S. ramosa*. This study suggests a much higher diversity of branching syllids than currently known. Finally, we discuss possible explanations for the feeding behaviour in the new species in relation to its highly ciliated wall of the digestive tubes (especially at the distal branches and anus), and provide a hypothesis for the evolution of branching body patterns as the result of an adaptation to the host sponge labyrinthic canal system.

Keywords Mitochondrial genome · Phylogenetics · Sponge · Syllidae · Symbiosis · Morphology · Anatomy · Ecology

✉ M. Teresa Aguado
aguadomolina@uni-goettingen.de

1 Biodiversitätsmuseum, Animal Evolution & Biodiversity, Georg-August-Universität Göttingen, Göttingen 37073, Germany

2 Departamento de Biología, Facultad de Ciencias, Universidad Autónoma de Madrid, Madrid 28049, Spain

3 Museum and Art Gallery of the Northern Territory, PO Box 4646, NT, Darwin 0801, Australia

4 Washington University in St. Louis, MO, St. Louis 63130, USA

5 Marine Biological Laboratory, MA, Wood Hole, 02543, USA

6 Misaki Marine Biological Station, School of Science, The University of Tokyo, Misaki, Miura, Kanagawa 238-0225, Japan

7 The National Institute of Advanced Industrial Science and Technology (AIST), Ibaraki, Tsukuba 305-8566, Japan

8 Marine Biological Station, Sado Island Center for Ecological Sustainability, Niigata University, 87 Tassha, Sado, Niigata 952-2135, Japan

9 Sesoko Station, Tropical Biosphere Research Center, University of the Ryukyus, 3422 Sesoko, Motobu-cho, Okinawa, 905-0227, Japan

10 Sugashima Marine Biological Laboratory, Toba, Sugashima 517-0004, Japan

Introduction

In 1879, McIntosh published the description of a "remarkable branched Syllid," *Syllis ramosa*, collected during the Challenger Expedition, one of the most significant natural history expeditions from the nineteenth century. The worms were found inside the hexactinellid sponge *Crateromorpha meyeri* (Gray, 1872) at 175 m deep near Cebu, in the Philippines. In relation to their lateral branches, McIntosh (1879) said: "the body of the annelid appears to have a furor for budding laterally, terminally, and wherever a broken surface occurs," which represented the first instance of an annelid species described with a randomly branching asymmetrical body. Some years later, in the complete report of marine annelids collected during the expedition, McIntosh (1885) described the same specimen of *S. ramosa*, together with another one found inside *C. meyeri* at 250 m deep close to the Kai Islands (Indonesia) in the Arafura Sea. Living specimens were found 10 years later by Oka (1895) (inside *C. meyeri* in Japan, around 25 km south of Misaki, between 550 and 730 m deep) and Izuka (1912) (in the "gastral cavity and adjacent parts" of *Crateromorpha meyeri rugosa* Ijima, 1898 in Sagami Bay at 180 m deep and in Suruga

Bay at 165 m deep, both in Japan). Later, another finding of a branching annelid from a distant geographic area (the northern Red Sea) was attributed to *S. ramosa* by Crossland (1933). However, it was found inside a small, fragile 10-mm diameter unidentified siliceous sponge attached to a dead coral [*Lobophyllia corymbosa* (Forsskål, 1775)] at 1.8 m deep and, unfortunately, no drawings or detailed descriptions were provided. Then, it was not until Read (2001) that another report of *S. ramosa* surfaced, this time from a specimen of *Crateromorpha* about 600 mm long found at 1000 m deep in the Tasman Sea of New Zealand. Unfortunately, the head was not found and no details about the chaetae were provided. Finally, Imajima identified as *S. ramosa* one specimen from Sagami Bay, found in 2005 at 36–50 m and deposited in the National Museum of Nature and Science of Tokyo (collection code: NSMT-Pol S; Catalogue number: 1568).

The second known branching species, *Ramisyllis multicaudata* Glasby et al., 2012, was described from the coastal shallows of Darwin, Northern Australia (Glasby et al., 2012). This study demonstrated notable differences in biology and morphology between this species and *S. ramosa* and analysed its phylogenetic relationships inside Syllidae. *Ramisyllis multicaudata* shares with *S. ramosa* a randomly branching asymmetrical body and its way of living inside the labyrinthic internal canals of sponges, but differs (except for the Red Sea and Imajima's 2005 Sagami Bay reports of *S. ramosa*) in the host sponge (*Petrosia vs. Crateromorpha*), depth (0–20 m *vs.* 100–1000 m deep), and key morphological and anatomical details. Both species reproduce by schizogamy, forming gamete-bearing posterior segments that develop typical stolon features like eyes and sensory appendages. Once formed, these stolons are detached from the stocks to swim freely in the water column, where spawning occurs, while the stocks regenerate the posterior end.

Combining different mitochondrial and nuclear genes, Aguado et al. (2015a, b) found that *R. multicaudata* was nested in a clade containing all Syllinae reproducing by gemmiparity [i.e., stolons being developed simultaneously from newly developed segments according to Franke (1999) and San Martín and Aguado (2014)]. The clade was informally named as "the ribbon clade" because most of its members show flattened bodies. Within it, *R. multicaudata* was the sister group of a clade with species of *Trypanobia*. The postembryonic addition of segments (typical of many annelids), together with the regenerative abilities of syllids and its ability to produce several simultaneous newly formed segments during gemmiparity, may be at the evolutionary basis of the development of a branching body in *R. multicaudata* (Aguado et al., 2015a, b). The complete mitochondrial genomes of *R. multicaudata* and *Trypanobia cryptica* Aguado et al. (2015b), showed a gene order considerably different to the ground pattern of Syllidae (Aguado et al., 2015a), the latter being similar to the putative ground pattern of Pleistoannelida (Aguado et al., 2016).

The present study describes a third species of branching syllid, the second within *Ramisyllis*, living inside an undescribed species of *Petrosia* found in shallow waters at Sado Island (Japan). We provide a detailed morphological study, a phylogenetic analysis including several mitochondrial and nuclear genes, genetic distance analyses, and the complete mitochondrial genome. We discuss the possible existence of other branching species, which may coexist in Japanese waters, and possible feeding strategies. Finally, we provide a hypothesis for the evolution of branching body patterns as an adaptation to live inside the labyrinthic canals system of their host sponges.

Materials and methods

Collection and morphological analyses

The specimens were collected on 1 October 2019 at Shukunegi Point (Sado Island, Japan, 37°48′17.1″N, 138°14′25.1″E) (Fig. 1). Collecting permits were obtained from the Ogi branch of the Sado fishery cooperative by the authors belonging to the Sado Marine Biological Station (SMBS) of The Niigata University. Twenty-five specimens of *Petrosia* with their symbionts were collected by SCUBA at 10–15 m deep (Online Resource 1). The habitat and sponges were photographed with an underwater camera (TG-5, Olympus). Each sponge was cut at its base with a diving knife, placed in a plastic zip bag containing sea water, brought to the SMBS (Fig. 1), and placed in trays with constantly running sea water, except five complete specimens which were directly preserved in formalin and later transferred into 100% ethanol. During the following four days, nineteen specimens were carefully dissected following Glasby et al. (2012). The remaining complete sponges were brought to Misaki Marine Biological Station (MMBS) of The University of Tokyo and placed in tanks with running sea water, where they survived for 3 months; three more sponges were dissected during this period. The worms were preserved in 100% ethanol, RNA later, methanol, formalin, paraformaldehyde (PFA) 4%, and phosphate-buffered saline pH 7.4 (PBS) for different purposes (Online Resource 1).

Morphological observations and photographs of branches, details of parapodia, stolons, and anterior ends were made using an Olympus SZX7 stereomicroscope and an Olympus BX53 compound microscope with attached cameras. For scanning electron microscopy (SEM), the specimens fixed in PFA 4% in PBS, were treated with OsO_4 for 20 min, rinsed with ddH_2O (five times), dehydrated in a graded ethanol series (20%, 50%, 70%, 90% 100%, 20 min each), critical point dried (in a BALZERS CPD 030), mounted on stubs, gold coated (with a BALZERS SCD 050), and observed and
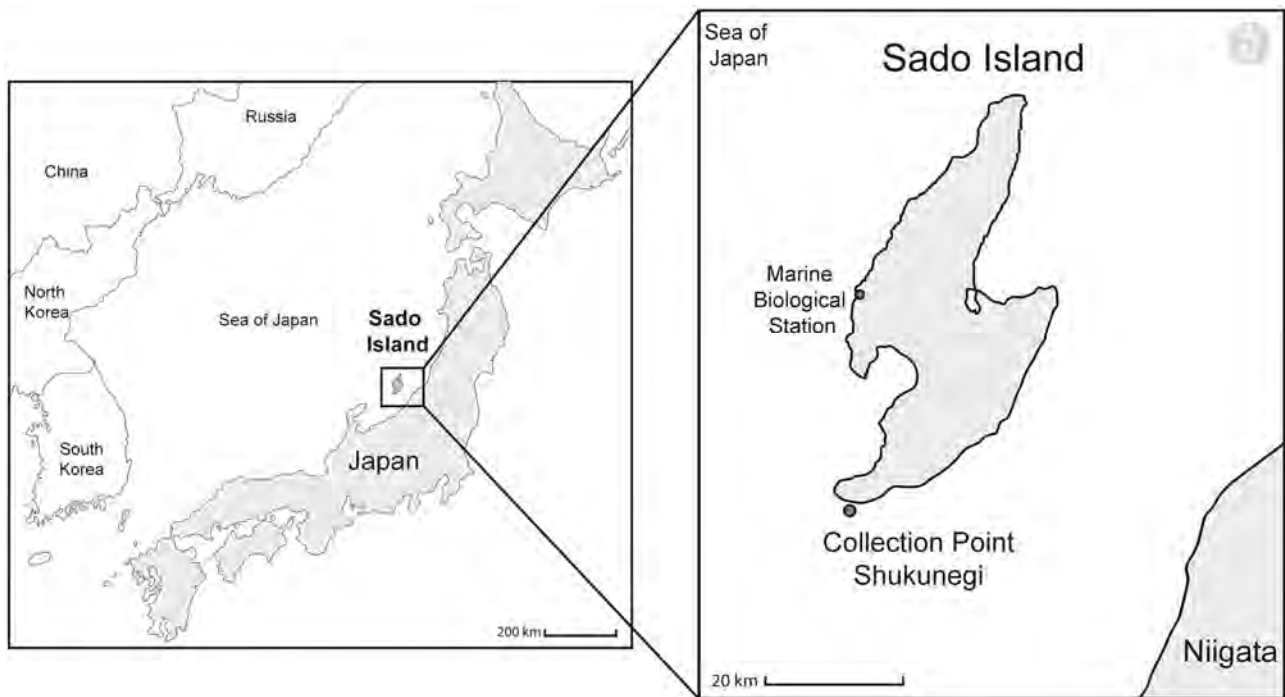
Fig. 1 Sampling area in the Sea of Japan. Shukunegi, Sado Island, Japan

photographed with a SEM FEI Quanta 250 FEG. Figures were prepared with Adobe Photoshop CC (Adobe).

The arrangement of the nervous-system was assessed by immunological staining using monoclonal antibodies against the general neuronal marker acetylated α-tubulin protein. Cell density and muscle disposition was assessed by staining with DAPI (4′,6-diamidino-2-phenylindole) and rhodamine-labelled phalloidin. Specimens fixed in 4% PFA in PBS were washed in 1XPBT (0.3% v/v Triton X-100 in 1XPBS), transferred to BBT (0.2% Bovine Serum Albumin in PBT), blocked for 30 min with NGS/BBT (2% v/v Normal Goat Serum in BBT), incubated overnight at 4 °C with the primary antibody (monoclonal Mouse anti-acetylated alpha-tubulin from AdipoGen, Seoul, Korea) in NGS/BBT (1:100 dilution), again washed in BBT and blocked with NGS/BBT, incubated in BBT (dilution 1:200) with the fluorescent-conjugated secondary antibodies (Alexa Flour 488 Goat anti-Mouse IgG, Invitrogen, Eugene, OR), washed in PBT, stained with rhodamine-labelled phalloidin (5 unit/mL PBT) or DAPI (5 µg/mL PBT), washed again with PBT, mounted with anti-fade solution VECTOR Shield (Vector Laboratories, Inc., Burlingame, CA), and observed using a confocal laser scanning microscope (FV3000, OLYMPUS, Tokyo). Image stacks were processed using Imaris 9.3 (Bitplane) and images were edited using Photoshop CC.

Type and voucher specimens have been deposited at the Biodiversitätsmuseum Georg-August-Universität Göttingen (ZMUG), the Museo Nacional de Ciencias Naturales de Madrid (MNCNM), and the National Museum of Nature and Science of Tokyo (NSMT).

DNA extraction, amplification, and sequencing

Seven specimens fixed in 90–100% ethanol and RNAlater were sequenced, together with seven specimens of *R. multicaudata* from Darwin (Australia) collected in 2009, 2015, and 2017 and fixed in RNAlater (Glasby et al., 2012; Ponz-Segrelles et al., 2021) (Table 1). Adequately fixed material is still not available for *S. ramosa*. Hence, this species has not been included in the phylogenetic and genetic distance analyses.

Genomic DNA was extracted using standard protocols from six of the seven specimens from each location and used to sequence the mitochondrial genes *cytochrome oxidase subunit 1* (*COI*) and *16S*, the nuclear genes *18S* and *28S*, and the nuclear marker *ITS2*. The remaining specimens from Japan (holotype, SA1; Table 1) and Darwin (RM7, Table 1) were used for genome and transcriptome sequencing, respectively (see methods below).

Single markers were obtained by polymerase chain reaction (PCR). Amplification consisted of an initial denaturation at 96 °C for 1–2 min, followed by 35–40 cycles of denaturation at 95 °C for 30 s to 1 min, annealing at 42–51 °C for 30 s and extension at 72 °C for 1–1.5 min. At the end of the reaction, a final extension of 8–10 min at 72 °C was performed. *COI* and *16S* sequences were

Table 1 Terminals included genes, GenBank accession numbers, and sampling localities. Sequences obtained for this study in bold

| Species	18S	16S	COI	28S	IST2	Locality
*Ramisyllis multicaudata*_RM1	KR604716	KR534502	KR534502	**OK172175**	-	Darwin, NT, Australia
*Ramisyllis multicaudata*_RM2	**OK169527**	**OK169536**	**OK166784**	**OK172172**	-	Darwin, NT, Australia
*Ramisyllis multicaudata*_RM3	**OK169528**	**OK169538**	**OK166786**	**OK172176**	-	Darwin, NT, Australia
*Ramisyllis multicaudata*_RM4	**OK169525**	**OK169540**	**OK166787**	**OK172173**	-	Darwin, NT, Australia
*Ramisyllis multicaudata*_RM5	**OK169526**	**OK169537**	**OK166783**	**OK172174**	-	Darwin, NT, Australia
*Ramisyllis multicaudata*_RM6	**OK169524**	**OK169539**	**OK166785**	**OK172178**	-	Darwin, NT, Australia
*Ramisyllis multicaudata*_RM7	**OK169523**	**OK169541**	**OK166788**	**OK172177**	**OK169529**	Darwin, NT, Australia
*Ramisyllis kingghidorahi*_SA1	**OK169520**	**MZ571475**	**MZ571475**	**OK172171**	**OK169531**	Sado Island, Niigata, Japan
*Ramisyllis kingghidorahi*_SA9	**OK169517**	**OK169511**	**OK156179**	**OK172167**	**OK169535**	Sado Island, Niigata, Japan
*Ramisyllis kingghidorahi*_SA28	**OK169519**	**OK169514**	**OK156177**	**OK172168**	**OK169534**	Sado Island, Niigata, Japan
*Ramisyllis kingghidorahi*_SA46	**OK169518**	**OK169515**	**OK156180**	**OK172165**	-	Sado Island, Niigata, Japan
*Ramisyllis kingghidorahi*_SA53	**OK169521**	**OK169513**	**OK156178**	**OK172166**	**OK169530**	Sado Island, Niigata, Japan
*Ramisyllis kingghidorahi*_SA87	**OK169516**	**OK169510**	**OK156181**	**OK172169**	**OK169532**	Sado Island, Niigata, Japan
*Ramisyllis kingghidorahi*_SA88	**OK169522**	**OK169512**	-	**OK172170**	**OK169533**	Sado Island, Niigata, Japan
Alcyonosyllis phili	KM277824	KM277822	KM277827	-	-	Kimberley, WA, Australia
Branchiosyllis exilis 1	JF903583	JF903692	-	-	-	Darwin, NT, Australia
Eurysyllis sp. A1	-	-	KX084930	KX084804	-	Balayan Bay, Luzon Island, Philippines
Eurysyllis sp. B1	KX084850	KX084862	KX084943	-	-	Sombrero Island, Balayan Bay, Luzon Island, Philippines
Eurysyllis tuberculata 4	KX084853	KX084925	KX084932	KX084806	-	Balayan Bay, Luzon Island, Philippines
Eurysyllis tuberculata 3	KX084851	-	KX084934	KX084807	-	San Vicente do Mar, Galicia, Spain
Eurysyllis tuberculata 1	JF903594	-	JF903787	-	-	Shark Bay, WA, Australia
Eurysyllis tuberculata 2	EF123833	-	EF123748	-	-	Banyuls-sur-mer, France
Eusyllis blomstrandi	EF123887	EF123788	EF123749	-	-	Kaldbak, Faroe Islands
Haplosyllis spongicola	EF123837	EF123791	EF123751	-	-	Banyuls-sur-mer, France
Megasyllis inflata	JF913966	JF913954	JF903776	-	-	Port Jackson, NSW, Australia
Parahaplosyllis brevicirra	-	JF903706	JF903784	-	-	Port Jackson, NSW, Australia
Parahaplosyllis kumpol	-	KX084922	KX084966	-	-	Cavalli Islands, New Zealand
Paraopisthosyllis alternocirra	JF903623	JF903707	JF903786	-	-	Rottnest Is., WA, Australia
Plakosyllis sp.	KX084855	-	KX084933	KX084808	-	El Nido, Palawan Island, Philippines
Pseudosyllis brevipennis 1	-	KX084917	KX084969	-	-	Port de la Selva, Girona, Spain
Pseudosyllis brevipennis 2	EF123878	EF123816	EF123785	-	-	Port de la Selva, Girona, Spain
Syllis amica	KX084858	KX084924	KX084927	KX280928	-	Puerto Colera, Girona, Spain
Typosyllis anoculata	DQ790098	-	-	DQ790071	-	GenBank
Syllis columbretensis	KX084845	KX084860	KX084928	KX280925	-	Cap de Creus, Girona, Spain
Syllis compacta	EF123846	EF123806	EF123772	-	-	Altea, Alicante, Spain
Syllis gracilis complex Sg1	KX281029	KX280967	KX281005	KX280926	-	"Koala point," Balayan Bay, Luzon Island, Philippines
Syllis gracilis complex Sg5	KX281030	KX280966	KX281007	KX280927	-	"Koala point," Balayan Bay, Luzon Island, Philippines
Syllis gracilis complex Sg10	KX281044	KX280937	KX280980	KX280920	-	El Nido, Palawan Island, Philippines
Syllis gracilis complex Sg9	KX281039	KX280936	KX280979	KX280919	-	"Mainif point" between Balayan Bay and Batangas Bay, Luzon Is, Philippines
Syllis hyalina	KX281051	-	KX280977	KX280931	-	Sombrero Island, Balayan Bay, Luzon Island, Philippines
Syllis lutea	JF903663	JF903736	JF903785	-	-	Shark Bay, WA, Australia
Syllis malaquini	MN533981	MN533980	MN533982	-	-	Aquarium Madrid, Spain
Syllis marugani	EF123863	EF123812	EF123780	-	-	Manazuru Peninsula, Japan
Syllis picta	KX281028	KX280968	KX281009	KX280924	-	"Twin Rocks," El Nido, Palawan Island, Philippines
Syllis pulvinata	KX281050	KX280969	KX280976	KX280929	-	Puerto Colera, Girona, Spain

Table 1 (continued)

| Species	18S	16S	COI	28S	IST2	Locality
Syllis ypsiloides Sg 19	KX281035	KX280970	KX280985	KX280916	-	"Mainif point," between Balayan Bay and Batangas Bay, Luzon Island, Philippines
Syllis ypsiloides Sg20	KX281032	KX280971	KX280989	KX280913	-	Easter Island, Chile
Syllis variegata	KX281049	KX280974	KX281010	KX280930	-	"Polpollcan," El Nido, Palawan Island, Philippines
Trypanedenta gemmipara	-	KX084920	-	-	-	Cavalli Islands, New Zealand
Trypanedenta gigantea	KX084842	KX084919	KX084947	-	-	Elephant Island, Antarctica
Trypanobia asterobia	-	MG053190	MG053197	-	-	Japan
Trypanobia cryptica	KR604717	KR534503	KR534503	**OK172164**	-	Lizard Island, Australia
Trypanospina martini	MG053194	MG053191	MG053200	-	-	"Mainif point," between Balayan Bay and Batangas Bay, Luzon Island, Philippines
Trypanosyllis aeolis	KX084817	KX084913	KX084968	-	-	El Toro Island, Mallorca, Spain
Trypanosyllis californiensis	KX084821	KX084869	KX084938	KX084812	-	La Jolla, San Diego, California
Trypanosyllis cristoboi	KX084818	KX084914	KX084935	-	-	"Sepok point," between Balayan Bay and Batangas Bay, Luzon Island, Philippines
Trypanosyllis depressa	KR364795	KR364797	KR364801	-	-	Lizard Island, Australia
Trypanosyllis estebani	MG053195	MG053193	MG053199	-	-	Banyuls-sur-mer, France
Trypanosyllis kalkin	-	KX084880	KX084970	-	-	Las Cruces, Valparaíso Region, Chile
Trypanosyllis cf. *krohnii* Tk6	KX084831	KX084878	KX084952	-	-	Port Jackson, NSW, Australia
Trypanosyllis cf. *krohnii* Tk12	KX084823	KX084881	KX084940	KX084814	-	Itapua Beach, Bahgo, Brazil
Trypanosyllis cf. *krohnii* Tk41	KX084833	KX084884	KX084957	-	-	"Beatrice Point," Sombrero Island, Balayan Bay, Luzon Island, Philippines
Trypanosyllis cf. *krohnii* Tk38	-	-	KX084941	KX084815	-	Maunalaya Bay Beach Park, South Shore of Oahu, Hawaii
Trypanosyllis krohnii	-	EF123817	EF123786	-	-	Banyuls sur Mer, France
Trypanosyllis leivai_1	-	KX084874	KX084942	KX084816	-	Philippines
Trypanosyllis leivai_2	KX084827	KX084876	KX084953	-	-	"Beatrice Point," Sombrero Island, Balayan Bay, Luzon Island, Philippines
Trypanosyllis luquei	-	-	KX084991	-	-	Anza Cove,SanDiego, California
Trypanosyllis luzonensis Tluzo19	KX084840	KX084908	KX084964	-	-	"Sepok point," between Balayan Bay and Batangas Bay, Luzon Is, Philippines
Trypanosyllis luzonensis Tluzo1	KX084838	KX084892	KX084963	-	-	Hong Kong University of Science and Technology, Hong Kong, China
Trypanosyllis sanchezi	MG053196	MG053192	MG053198	-	-	El Cachucho MPA, Cantabrian Sea, Spain
Trypanosyllis sp.	KX084818	KX084914	KX084935	KX084809	-	Sepok Point, Between Balayan Bay and Batangas Bay, Luzon Is, Philippines
Trypanosyllis taboadai	KX084819	KX084866	KX084936	KX084810	-	Cavalli Islands, New Zealand
Typosyllis antoni	MN545360	NC_031404	NC_031404	-	-	Aquarium Leipzig, Germany
Typosyllis edensis	JF903658	JF903732	JF903789	-	-	New Port, NSW, Australia
Typosyllis gerundensis	KX084847	KX084861	KX084929	-	-	El Toro Island, Mallorca, Spain
Xenosyllis moloch	KX084857	KX084916	KX084944	-	-	Koala point," Balayan Bay, Luzon Island, Philippines
Xenosyllis scabroides	JF913974	JF903753	-	-	-	Lizard Island, QLD, Australia

obtained with the primers from Folmer et al. (1994) and Simon et al. (1994), respectively. For *18S*, *28S*, *ITS2*, and extending *COI*, new specific primers for *Ramisyllis* were designed with CLC Genomic Workbench 20 (Online Resource 2). The products of successful amplification were purified using ExoSAP-IT PCR Product Cleanup protocol (ThermoScientific). Sequences were revised with BioEdit (Hall, 1999) and CodonCodeAligner (CodonCode, Dedham, MA, USA).
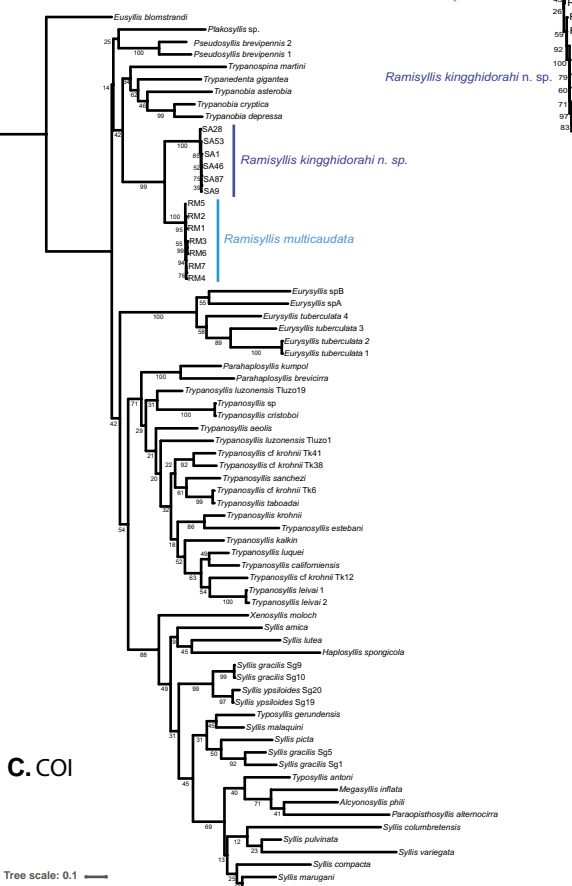
Sequences of other species of Syllinae used in the phylogenetic analyses were obtained from GenBank and selected based on the maximum number of available genes (*COI*, *16S*, *18S*, and *28S*) (Table 1). The analysis included representatives of the main groups previously identified as
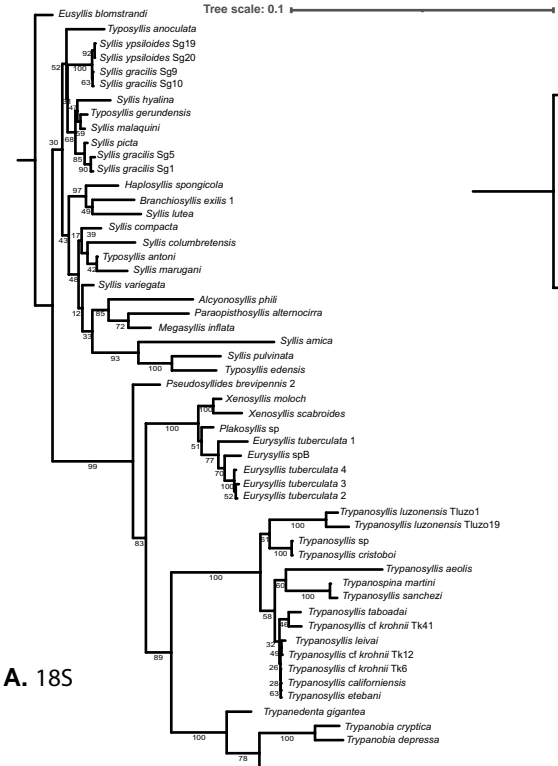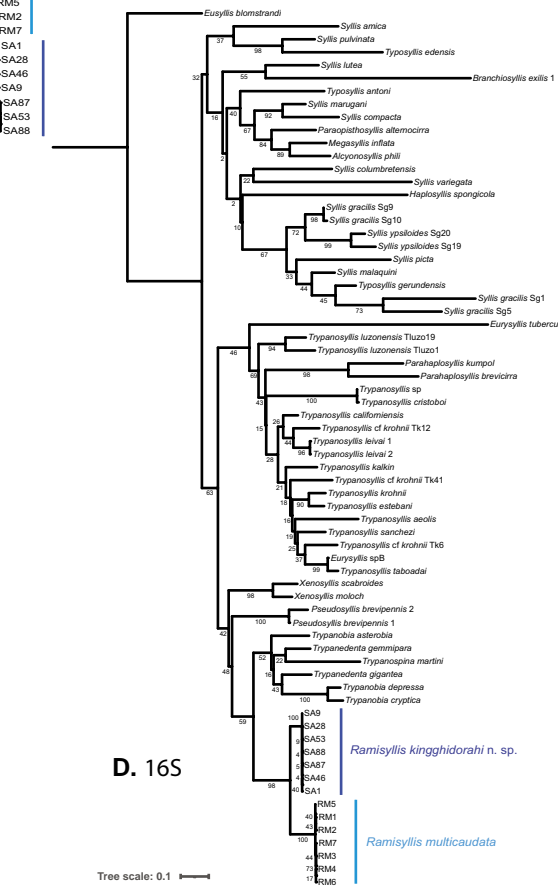
A. 18S
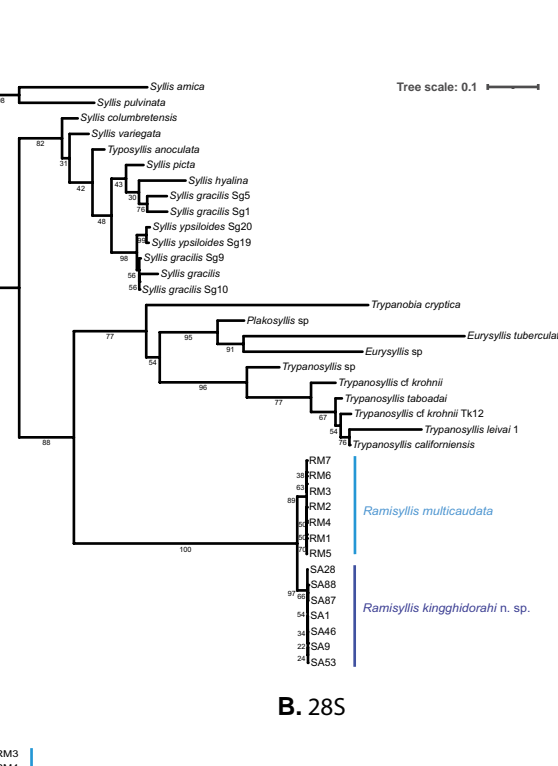
B. 28S

C. COI

D. 16S

◄**Fig. 2** Maximum likelihood trees. **A** Tree obtained when analysing *18S* data set. **B** Tree obtained when analysing *28S* data set. **C** Tree obtained when analysing *COI* data set. **D** Tree obtained when analysing *16S* data set. Bootstrap support values below nodes. *Syllis* and *Typosyllis* species as they were originally described

closely related to *R. multicaudata* (Aguado et al., 2015a), and the main groups within Syllinae (Aguado et al., 2012; Ribeiro et al., 2020). The Eusyllinae *Eusyllis blomstrandi* (Malmgren, 1867) was used as the outgroup.

Genome sequencing and analyses

For Illumina sequencing, double index sequencing libraries with average insert sizes of around 300 bp were prepared (Meyer & Kircher, 2010). The libraries were sequenced as 125 bp paired-end run, on an Illumina Hi-Seq 2000. Base calling was performed with freeIbis (Renaud et al., 2013), adaptor and primer sequences were removed using lee-Hom (Renaud et al., 2014), and reads with low complexity and false paired indices were discarded. The quality of all sequences was checked using FastQC v.0.11.5 (RNA data) and v.0.11.9 (DNA data) (http://bioinformatics.babraham.ac.uk/projects/fastqc/). Raw data of all libraries were filtered by removing all reads that included more than 5 bases with a quality score below 15. De novo genome assemblies were conducted with SPAdes 3.15.2 and IDBA-UD 1.1.046 (Peng et al., 2012; Prjibelski et al., 2020) using an initial k-mer size of 21, an iteration size of 10, and a maximum k-mer size of 81. N50 and average GC-content of genome assemblies were evaluated using QUAST v.5.0.2 (Gurevich et al., 2013). All sequence data were submitted to the Sequence Read Archive of the National Centre for Biotechnology Information (NCBI-SRA) (Table 1).

For transcriptome data, Trimmomatic v.0.38 (Bolger et al., 2014) was used after sequencing to trim and filter low quality reads with the options ILLUMINACLIP HEADCROP:10 LEADING:20 SLIDINGWINDOW:5:20 MINLEN:70. The surviving trimmed reads were used for de novo transcriptome assembly of *R. multicaudata* using Trinity 2.4.0 (Grabherr et al., 2011; Haas et al., 2013).

In the obtained genome assembly of the Japanese *Ramisyllis* SA1, the *18S* and *28S* gene sequences were identified using BLASTN (Altschul et al., 1990; Zhang et al., 2000) searches with the sequences of *18S* from *R. multicaudata* (KR04716) and *28S* of *Typosyllis anoculata* (Hartmann-Schröder, 1962) (DQ790071) as query. *COI* and *16S* gene sequences were obtained from the assembled mitochondrial genome (see below). *COI*, *16S*, and *18S* sequences of *R. multicaudata* (KR534502, KR04716) from Aguado et al. (2015a) were used to identify these gene sequences in the new transcriptome of the Darwin *R. multicaudata* RM7. The *28S* gene sequence found in the assembly of the Japanese

specimen was used as query to search for homologous sequences in the assembled transcriptome of *R. multicaudata*, as well as in the previously available assemblies of *T. cryptica* and *R. multicaudata* (Aguado et al., 2015a).

The *ITS2* marker was identified in the obtained genome and transcriptome using the available cluster *ITS1-5.8S-ITS2-28S* from *Proceraea cornuta* (Agassiz, 1862) (AF212165) and used to estimate genetic distances.

Mitochondrial genome annotation and analyses

The complete mitochondrial genome (mt-genome) of the Japanese holotype SA1 (Table 1) was identified using BLASTN searches with the mt-genome of *R. multicaudata* (KR534502) (Aguado et al., 2015a) as query. Mt-genome annotation and prediction of secondary structure of tRNAs and rRNAs were performed using MITOS webserver (Bernt et al., 2012) with the invertebrate mitochondrial code (NCBI code) (Online Resource 3). All automatic annotations were edited manually. Circular mt-genome representation was obtained with GenomeVx (Conant & Wolfe, 2008).

AT and GC skew were determined for the complete mitochondrial genomes (plus strand) according to the formula AT skew $= (A - T)/(A + T)$ and GC skew $= (G - C)/(G + C)$, where the letters stand for the absolute number of the corresponding nucleotides in the sequences (Perna & Kocher, 1995). Characterization of codon usage bias was calculated with DAMBE7.2.152 (Xia, 2018) (Online Resource 4).

Phylogenetic analyses

Each marker was aligned separately using the MAFFT v7 online tool (Katoh & Standley, 2013; Katoh et al., 2017) with default parameters and gap open and extension values, and using the iterative refinement method E-INS-i. Alignments were manually checked using Bioedit v7.2 (Hall, 1999) and AliView v1.27 (Larsson, 2014). Ambiguously aligned *18S* regions were checked and slightly manually improved based on a *18S* alignment performed only with sequences of *Ramisyllis*. All alignments are available at TreeBASE (https://www.treebase.org/). Single genes (*COI*, *16S*, *18S*, *28S*) were concatenated using FASconCAT-G (Kück & Longo, 2014; Kück & Meusemann, 2010). Maximum Likelihood (ML) tree inference of each gene was analysed with IQ-TREE v1.6.12 (Chernomor et al., 2016; Nguyen et al., 2015), and best fitting models were selected with the IQ-TREE embedded instance of Modelfinder (Kalyaanamoorthy et al., 2017) (*COI*: TIM2+F+I+G4; *16S*: TIM2+F+G4; *18S*: TN+F+I+G4; *28S*: TN+F+G4). Tree inference with the concatenated matrix (*COI*+*16S*+*18S*+*28S*) was also performed with IQ-TREE in a similar way. In all analyses, each partition was allowed to have its own set of branch lengths
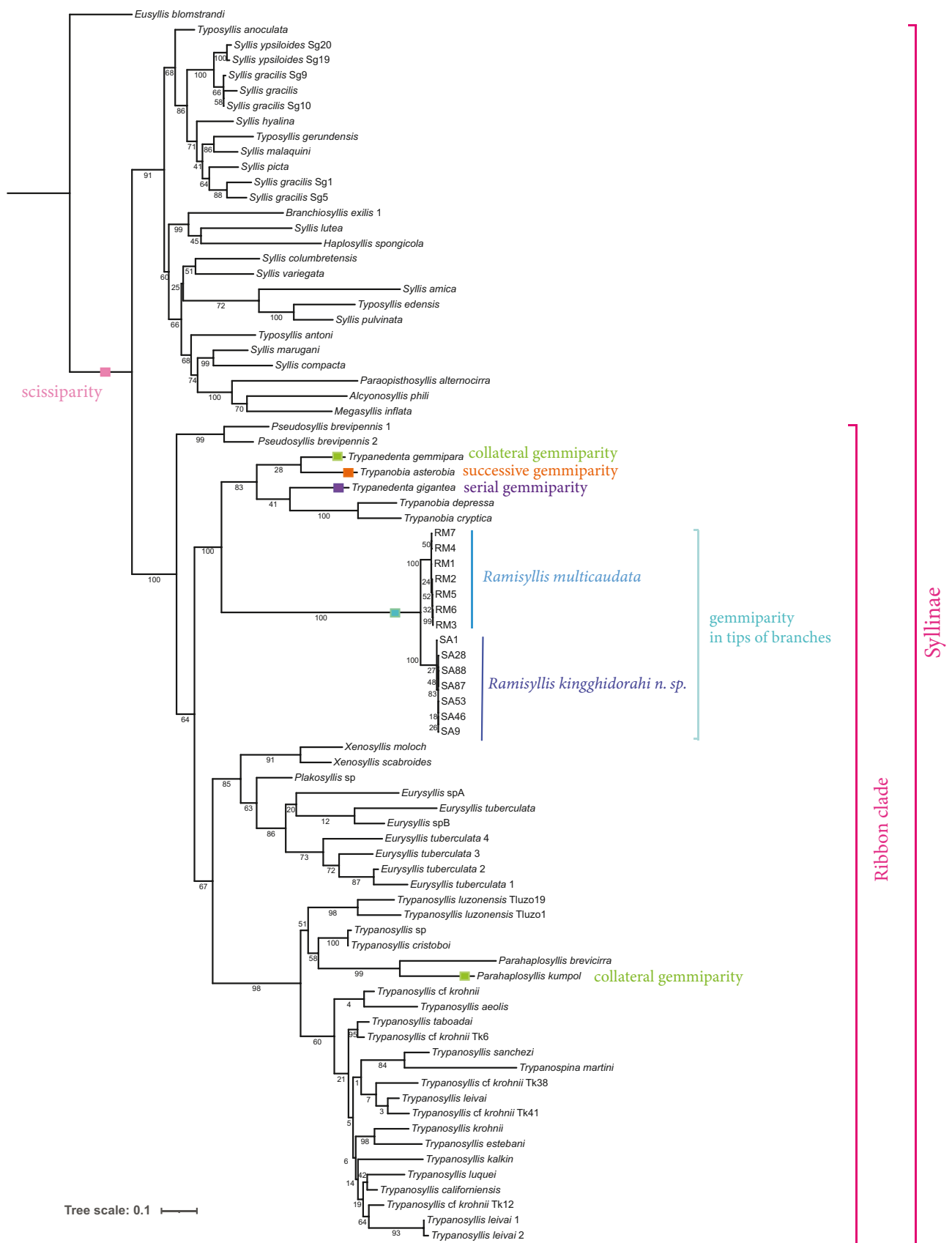
Fig. 3 Maximum likelihood tree obtained when analysing the concatenated data matrix (*28S + 18S + COI + 16S*). Bootstrap support values below nodes. *Syllis* and *Typosyllis* species as they were originally described

Fig. 4 Circular representation of the mitochondrial genome of *Ramisyllis kingghidorahi* n. sp

(-sp option). Support values were estimated based on 1000 bootstrap pseudo replicates (B).

Genetic distances and species delimitation

Genetic distances were only estimated for those species that were phylogenetically closer to *Ramisyllis*. Terminals with incomplete genes (e.g., only one or two of the three sequencing regions of *18S* or *28S*, or incomplete *COI* and/or *16S*) were excluded. Alignments were made with MAFFT v7

and MUSCLE (Madeira et al., 2019). Ambiguously aligned and variable regions in the alignments were recognized and excluded using Gblocks (Castresana, 2000) with relaxed parameters (smaller final blocks, gap positions within the final blocks, and less strict flanking positions allowed). For *16S* and *COI*, within country variability was better assessed using alignments including only sequences of *Ramisyllis*. For *28S* and *18S*, alignments with only *Ramisyllis* sequences were considered since the available information for the other terminals only recovered a small portion of *28S* and, in the

alignment of 18S with the rest of the syllines, the regions that remained after excluding ambiguously aligned positions included only the conserved blocks where the variability among *Ramisyllis* sequences was too low. For *ITS2*, only sequences of *Ramisyllis* were analysed since no other *ITS2* sequence data is available for Syllinae. Nucleotide divergence over sequence pairs (p-distance and best fitting substitution model; Online Resources 5–10) was estimated in MEGA v.7 (Kumar et al., 2016).

Results

Phylogenetic results

The *18S* and *28S* sequences of *Ramisyllis* from Australia and Japan differed considerably from those of all other syllids. *18S* showed insertions in regions V2 and V5 (which were especially difficult to align), while for *28S* there are still few available sequences. Moreover, only our *28S* sequences (both for *Ramisyllis* and *T. cryptica*) are complete, while most others available in Genbank represent only a short region (300–500 bp).

All *COI*, *16S*, *18S*, and *28S* trees (Fig. 2), as well as those from the concatenated data matrix (*COI* + *16S* + *18S* + *28S*) (Fig. 3) were congruent. In the *COI*, *16S* and *28S* ML tree inference analyses, the sequences of *Ramisyllis* (seven from Australia and seven from Japan) are organized in two well-supported sister clades (Figs. 2 and 3), with some structure within each clade being detected in *COI* and *16S* (Fig. 2c, d) and no clear within-clade differences for *28S* (Fig. 2b). In *16S*, *28S*, and, especially, *COI*, the branch length of each clade is long enough to recognize the Australian and Japanese groups (Fig. 2b–d), while in *18S*, the within-clade branches are extremely short and the Japanese clade is nested within the Australian one, revealing few variations (Fig. 2a). In contrast, the branch length joining *Ramisyllis* with its sister group *Trypanobia-Trypanedenta* is considerably long in *18S* (Fig. 2a) and *28S* (Fig. 2b), whereas it is average when compared to other branch lengths within Syllinae for *16S* and *COI* (Fig. 2c, d).

The *Ramisyllis* clade is nested within the "ribbon clade" (sensu Aguado et al., 2015a) in all inferred phylogenies and appears as sister group to *Trypanobia* and *Trypanedenta* clade (83B) in the concatenated data analysis (Fig. 3). The "ribbon clade" is always well supported but, in the concatenated data analysis, it shows an early subdivision in a well-supported (99B) small clade (*Pseudosyllis brevipennis* Grube, 1863 specimens) and a less-supported (64B) large clade including the remaining genera and species. Within this one, a large clade (67B) shows a dichotomy between the *Xenosyllis-Plakosyllis-Eurysyllis* clade (85B) and *Trypanosyllis-Parahaplosyllis* (98B). *Eurysyllis*, *Xenosyllis* and *Parahaplosyllis*, all represented by more than one species, are monophyletic, whereas *Trypanosyllis* appears as paraphyletic.

Mitochondrial genome

The complete mitochondrial genome of the Japanese *Ramisyllis* SA1 (Tables 1, S1) was identified in a single contig among the sequences of the assembled low-coverage genome. It is 16.517 bp long (longer than in *R. multicaudata*) and AT-rich (67%). A is the most common base (34%), and G the least common (12%). The coding strand has a strong skew of G *vs.* C (-0.313), whereas the AT skew is positive (0.034). The mt-genome contains 37 genes (13 protein-coding genes, two rRNA genes, and 22 tRNA genes) as in most other annelids and typically present in bilaterian mt-genomes (Online Resource 3).

Gene arrangement did not differ between the Japanese and Australian *Ramisyllis* (Aguado et al., 2015a) (Fig. 4). The mt-genome of the Japanese *Ramisyllis* has a 821 bp long putative control region flanked by nad6 and trnL1 and 25 non-coding regions ranging from one to 320 bp, with the largest one between trnT and rrnD (Fig. 14; Online Resource 3). ATG and TAA are the start and stop codons for all 13 protein coding genes (Online Resource 3). There is also a marked codon usage bias (Online Resource 4), with NNGs being the least used, and NNTs and, especially NNAs being the most common. The ribosomal RNAs are 1011 bp long for *16S* (*rrnL*), and 795 bp long for *12S* (*rrnS*). The two genes are only separated by an intergenic spacer of 20 bp (Online Resource 3). As in the Australian *Ramisyllis* (Aguado et al., 2015a), the DHV stem is missing in *trnC* and *trnR*, while shortened in *trnS1*. In contrast, while the DHV stem in *trnS2* is shortened in *R. multicaudata* from Australia, it is longer in *Ramisyllis* from Japan.

Genetic distances

COI genetic distances between Australian and Japanese *Ramisyllis* are 20–21% based on a Tajima-Nei model and 17–18% based on p-distances (Online Resource 5), while the within-clade divergence is 1% and that between the *Ramisyllis* clade and other species of the "ribbon clade" range
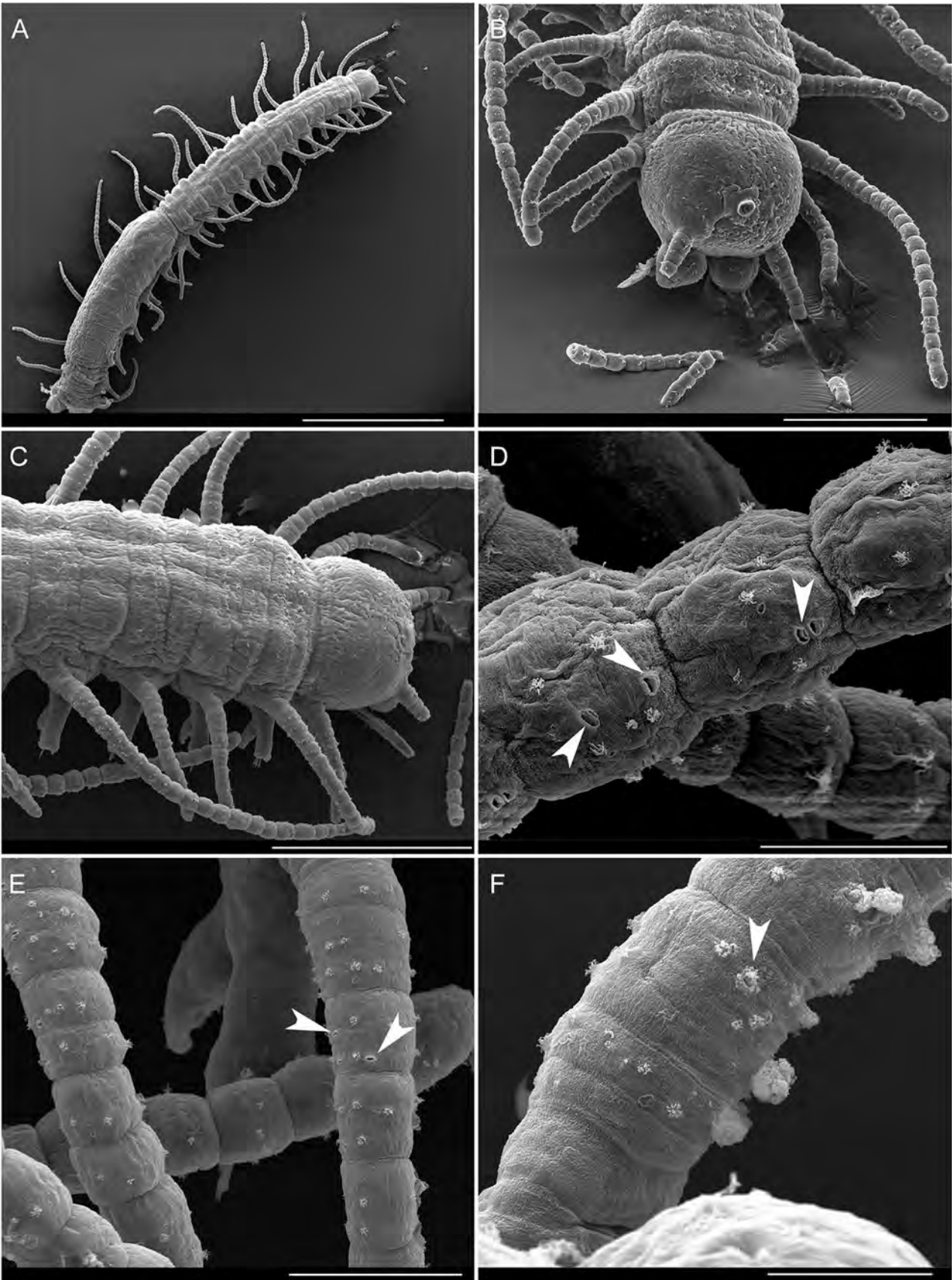
between 26 and 40% (Online Resource 6). Several species of *Trypanosyllis* show distances of 17–26% between them (in yellow in Online Resource 6). *Trypanedenta gemmipara* (Johnson, 1901), *Trypanedenta gigantea* (McIntosh, 1885), and *Trypanobia asterobia* (Okada, 1933) show distances of 16% among them. The *16S* genetic distance between the Australian and Japanese *Ramisyllis* ranges between 10 and 11% based on Tajima-Nei model (Online Resource 7), while it is 0–1% within-clades. Distances obtained when analyzing the alignment including only *Ramisyllis* sequences (not shown) are the same as those obtained in the alignment with the rest of the "ribbon clade" species (Online Resource 7). The distance with other species in the ribbon clade ranges between 25 and 33% and some species of *Trypanosyllis* show distances of 11–15% (in yellow in Online Resource 7). In *28S*, the genetic distance between the Australian and Japanese specimens is 4% (Online Resource 8), while in *18S*, it is 1% (Online Resource 9), being the latter non-significant. In *ITS2*, the genetic distance between the Australian and Japanese specimens is 11% (Online Resource 10).

Taxonomy

Ramisyllis Glasby et al., 2012

Diagnosis (after Glasby et al. (2012), emendations in bold).

"Ribbon clade" Syllinae, with non-flattened body, more or less cylindrical segments and a **multiaxial**, dendriform pattern; first branch occurring after **segments 14–24**. **Branches emerging after parapodia (not replacing them or dorsal cirri) and showing same segment size and cirri length as previous branches**. Three antennae; palps free to base; two pairs of tentacular cirri; pharynx slender, mid-dorsal tooth absent in adults; dorsal cirri articulated, with alternating thick/slender pattern on mid-body and posterior segments; ventral cirri present, not articulated, inserted proximally; single type of simple chaeta present, tomahawk-shaped. **Sexes separate**. Reproduction by schizogamy, **gemmiparity**. **Acerous, dimorphic** stolons. **Commensal inside shallow water species of *Petrosia*. Mitochondrial gene order strongly modified. Nuclear ribosomal sequences highly derived compared to other Syllinae.**

Ramisyllis kingghidorahi n. sp. Aguado, Ponz-Segrelles, Glasby, Ribeiro, Jimi & Miura. Figures 5–14

urn:lsid:zoobank.org:act:5E809913-30EF-43A1-831C-F6CFED9B40E7.

Diagnosis

Species of *Ramisyllis*, sister-group related to *R. multicaudata*, long anterior tentacular and dorsal cirri (twice long as midbody ones), long proventricle (through 4 segments), stolon stalks similar to other segments in regular branches and proliferation of new branches in intersegmental areas.

Material examined

HOLOTYPE: Female (ZMUG 29,568, MNCNM 16.01/19089–90), samples SA1-SA6, 1 Oct 2019, 37°48′17.1″N, 138°14′25.1″E, 15 m deep, coll. Aguado, Ponz-Segrelles, Miura, Oguchi, Omori & Kohtsuka.

PARATYPES: Paratype 1: male (ZMUG 29,569, MNCNM 16.01/19091–92), samples SA7-22; paratype 2: male (ZMUG 29,571), samples SA28-34; paratype 3: non reproductive specimen (ZMUG 29,573, MNCNM 16.01/19093), samples SA43, 46; paratype 4: male (ZMUG 29,576), samples SA61-62; paratype 5: non reproductive specimen (ZMUG 29,576), sample SA63; paratype 6: male (ZMUG 29,583, MNCNM 16.01/19094–96), sample SA85-91; paratype 7: non reproductive specimen (ZMUG 29,585), sample 96; paratype 8: male (ZMUG 29,586), sample SA102; paratype 9: female (NSMT Pol-P-843), sample 220. All paratypes collected on 1st Oct 2019, 37°48′17.1″N, 138°14′25.1″E, 15 m deep, by Aguado, Ponz-Segrelles, Miura, Oguchi, Omori & Kohtsuka.

Additional material: 1 female (ZMUG 29,570), 1 male (ZMUG 29,572), 1 female (ZMUG 29,574), 1 male (ZMUG 29,578), 1 non reproductive specimen (ZMUG 29,579), 1 male (ZMUG 29,578), 1 female (ZMUG 29,582), 1 male (ZMUG 29,584), 1 male (ZMUG 29,589), 6 specs. (Sex not determined, undissected sponges with worms inside) (ZMUG 29,587, 29,590–94), male stolons (ZMUG 29,595, 29,598), female stolons (ZMUG 29,597). All specimens collected on 1st Oct 2019, 37°48′17.1″N, 138°14′25.1″E, 15 m deep, by Aguado, Ponz-Segrelles, Miura, Oguchi, Omori & Kohtsuka.

Comparative material

Ramisyllis multicaudata. Seven specimens (RM 1–7, Online Resource 2), Darwin Harbour, Channel Island (type locality), 12°33.2′S, 130° 52.4E′, coll. and identified by Glasby, Aguado & Ponz-Segrelles.

Syllis ramosa. 1 specimen University Museum of the University of Tokyo (UMUTZ-Ann-Pc-95) Found in the "gastral cavity and adjacent parts" of *Crateromorpha meyeri rugosa* in Sagami Bay (around 180 m deep). Coll. by K. Aoki and identified by A. Izuka (1912).

Syllis cf. *ramosa*. 1 specimen from the National Museum of Nature and Science of Tokyo (NSMT-Pol
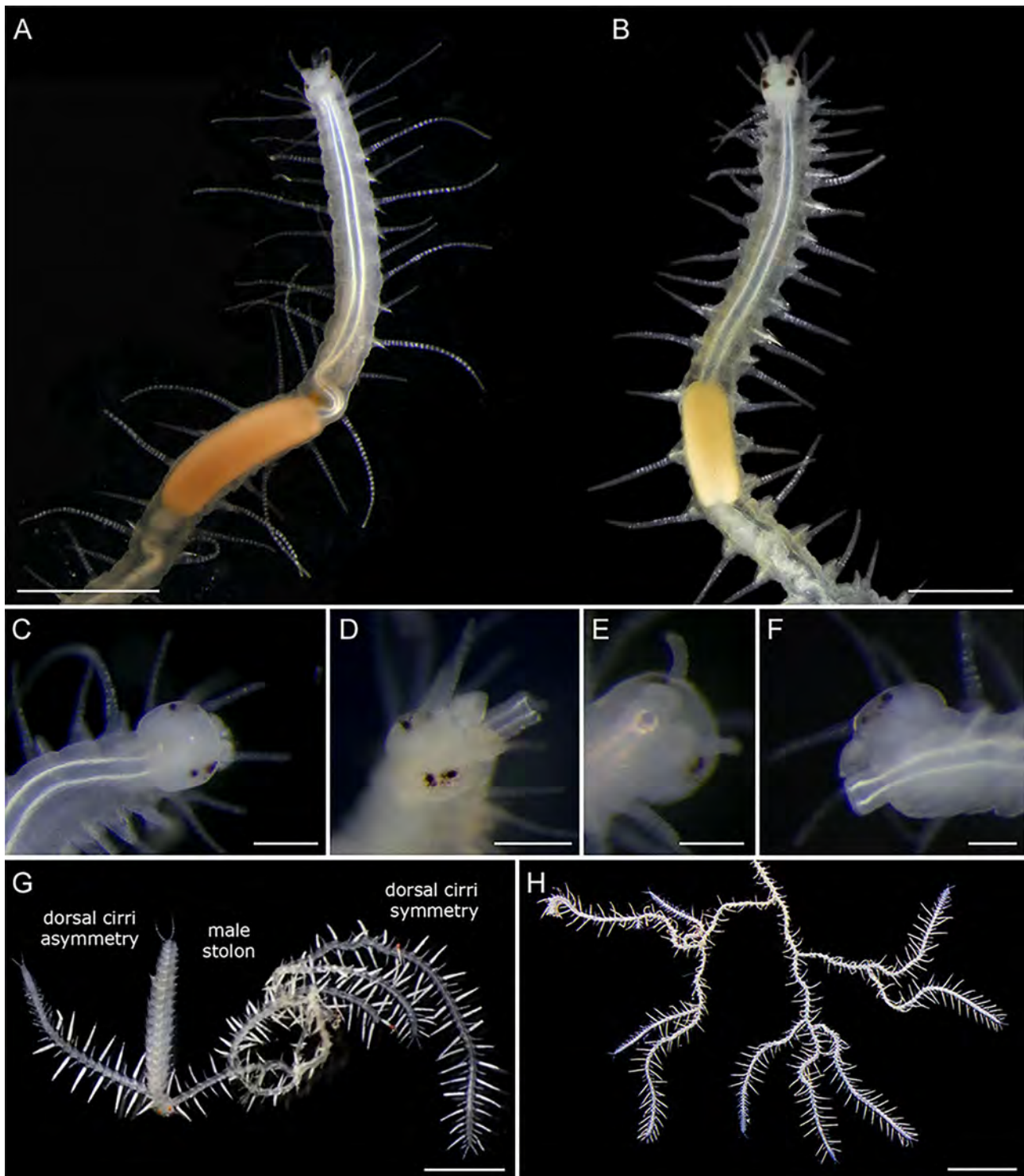
Fig. 7 Stereomicroscopy images of living specimens of *Ramisyllis kingghidorahi* n. sp. (**A, C-H**) and *Ramisyllis multicaudata* (**B**) for comparison. **A** *Ramisyllis kingghidorahi* n. sp. Holotype. **B** *R. multicaudata* anterior region, dorsal view; picture modified from Ponz-Segrelles et al. (2021), with permission. **C** Prostomium and first segments in detail, dorsal view. **D** Anterolateral view of prostomium with details of palps and pharynx everted. **E** and **F**. Pharynx everted in ventral view. **G** Branching asymmetries in dorsal cirri. **H** Branching asymmetries in body shape. Scale bars: 1 mm **A**, **B**, 200 µm **C**, **D**, 100 µm **E**, **F**, 2 mm **G**, **H**

S. 1568). Found in "a sponge" at Sagami Bay (around 35–50 m deep), collected and identified by M. Imajima in 2005.

Etymology

The name refers to King Ghidorah, the three-headed and two-tailed monster enemy of Godzilla. Both characters were created by Tomoyuki Tanaka based on Japanese mythology and folklore. King Ghidorah is a branching fictitious animal that can regenerate its lost ends. King Ghidorah is assumed to be a male and latinized accordingly.

Distribution and habitat

Coastal waters of Sado Island, Japan, around 15 m deep; symbiont of *Petrosia* sp. (pink form).

Ecology

The sponges were collected on vertical stone walls, slopes, or small caves, usually in less exposed areas where they were often accompanied by other sponges, encrusting algae, and coralline algae. The sponges measured 5–10 cm in diameter and were usually irregularly round and pink, with mostly smooth surfaces except some areas showing crests, dead and healed areas (Fig. 5c), and some large oscula (Fig. 5d). Immediately after placing the sponges in trays, many very active, fast-swimming male stolons (see description below) left them. After 2–3 h, swimming female stolons (see description below) also left, moving slower than males. Detached stolons, mostly males, shook vigorously (Video S1), as in other syllids (MTA, personal observation). Dissection revealed only one worm specimen per sponge, most of them developing stolons (ten were males, five females), though not all of them showed signs of stolonization (four specimens). In sponges containing sexually mature specimens with attached stolons, some fully developed, detached stolons were also found in the sponge canals. All attached and free stolons from the same sponge specimen were of the same sex.

The anterior worm end, considerably less active than the posterior ends, was always at the inner basal area of the sponge. No pattern was observed in the position or orientation of the branches. The sponges were generally widely occupied, particularly in some areas. Worm branches were quite flexible and elastic, which facilitated fluent movement within the canal system. However, even though some branches could move outside the sponge when needed, worms were not able to abandon the sponge, even when some of their branches were dying. In natural conditions, the posterior ends emerged from the ostia or the oscula only

in one specimen. In the laboratory, posterior ends moved on the sponge surface (Fig. 5e, f).

Description

External morphology Dendriform branching body with one anterior and multiple posterior ends (Fig. 5a, b). Random branching asymmetry (Fig. 7h). Body subcylindrical, ventrally flattened, mostly translucent (except some yellowish or brownish areas in vivo). Holotype 0.36 mm wide at proventricle level, without parapodia. Branches always dichotomous, emerging at approximately right angles from intersegmental areas (Fig. 9a–d). Paired branches from same segment not seen. Holotype with first branching point after segment 24, second 4 and 6 segments later on each respective branch (Fig. 5a). Number of segments between two contiguous ramifications lacking obvious branching pattern (4–10 segments in holotype anterior branches to 10–20 segments between branching points in other regions). Most midbody segments as long as wide (70 μm length) (Fig. 9a–c, e–f), with some areas with much longer segments, 2–3 times as long as regular ones (174 μm; Fig. 9d), rectangular, yellowish or brownish, with much shorter dorsal cirri (Fig. 9d).

Prostomium rounded, with two pairs of eyes, anterior pair larger than posterior one; antennae articulated, median one slightly longer (8 articles in holotype) than lateral ones (6–7 articles in holotype) (Figs. 6a–c and 7a, c–d). Median antenna placed behind lateral ones (Fig. 6b). Palps small, conical, ventrally directed (Fig. 6b). Nuchal organs absent (Fig. 6b, c). Tentacular cirri articulated, dorsal ones longer (11 articles in holotype) than ventral ones (7 articles in holotype) (Fig. 6b, c). Dorsal surface of segments anterior to proventricle with a transversal band of cilia (Fig. 6c), then with bunches of cilia in proventricular segments (Fig. 10i) and with minute crests on midbody segments in one specimen (Fig. 10e–g).

Dorsal cirri usually straight, stretched horizontally in life (Fig. 7h), articulated, with those in segments anterior to first branching point longer (23 articles in holotype) than remaining ones (11–15 articles in holotype) (Fig. 5a). Anterior dorsal cirri as: 1st long, 2nd short, 3rd short, 4th long, 5th short, 6th long, 7th short, 8th short, and 9th long; remaining dorsal cirri generally with a strong long-short alternation in length (6–11 vs. 3–7 articles) (Fig. 9e, f). Longer dorsal cirri wider than short ones (Fig. 8). Some midbody branches with long yellowish segments (see above) and dorsal cirri with 1–4 articles lacking clear length alternation (Fig. 9d). Dorsal cirri length and shape symmetrical on each segment, but symmetry occasionally lost (one long and one short dorsal cirrus on same segment) (Fig. 7g). Dorsal cirri with spiral glands, larger and more remarkable in long ones (Figs. 8a, c-e, and
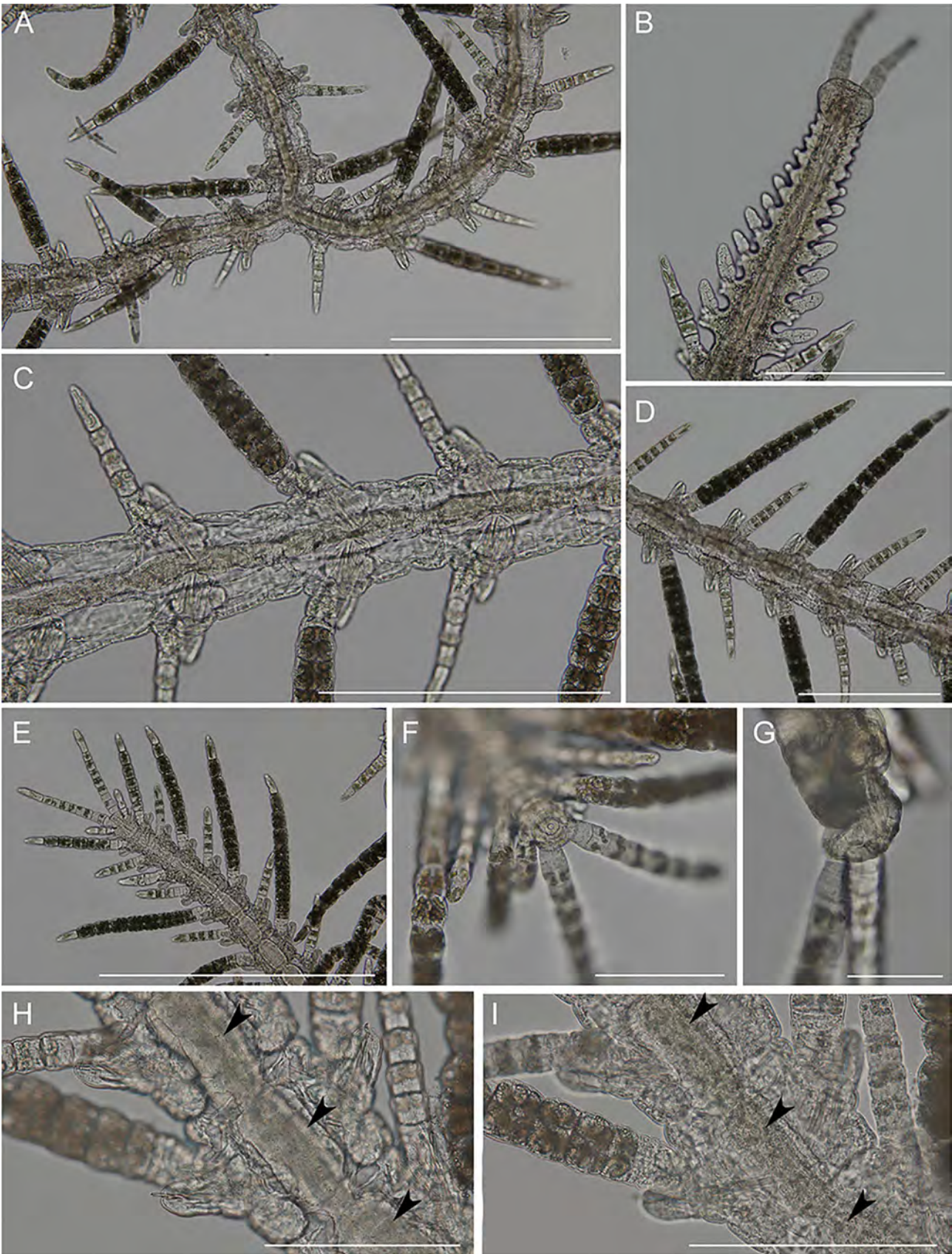
◀**Fig. 8** Light microscope images of living specimens of *Ramisyllis kingghidorahi* n. sp. **A** Branching point. **B**, **E–G** Posterior ends showing pygidia. **C**, **D**, **H**, **I** Midbody segments in regions of long dorsal cirri. Arrows point to the ventral blood vessel in **H** and the digestive tract in **I. A**, **D**, **E**, and **I** in dorsal view. **B**, **C**, **F** and **H** in ventral view. **G** In lateral view. Scale bars: 500 μm **A**, **E**, 200 μm **B**, **C**, **D**, 100 μm **F**, **H**, **I**, and 50 μm **G**

11a, c-f), opening exteriorly through both large and minute pores (joined in perforate plates) (Fig. 6d-f). Glandular content bright white in vivo, especially evident in long dorsal cirri (Fig. 7g), turning into intense red and massively protruding outside through pores when dying (Figs. 6g and 11b, f).

Ventral cirri short, unarticulated, digitiform to oval, basally inserted on parapodia, shorter than parapodial lobes, with numerous pores (Fig. 12g). Neuropodia bearing 2–3 simple chaetae (Fig. 12d-f), occasionally one (Fig. 12h), and one pointed acicula (Fig. 11g). Chaetae tomahawk shaped, bifid distally, prominent subdistal spur and series of denticles between teeth and spur; angle and relative sizes of distal teeth varies slightly along the body (Fig. 12a-f, h).

Pygidial cirri articulated, resembling dorsal cirri of posterior segments (9–10 articles) (Figs. 8e, f, and 10b). Numerous posterior ends regenerating with shorter dorsal and pygidial cirri (Fig. 10a). Anal openings densely ciliated (Fig. 10c, d).

Internal anatomy Alimentary canal visible by transparency (Fig. 8a, c, i). Pharynx slender, through 12 segments in holotype, about one-fourth width of proventricle (Figs. 5a, 7a). Long, slender, cylindrical, strongly-cuticularized, with no tooth or trepan, partially eversible (Figs. 7d–f). Pharynx mostly straight, with a curve anterior to proventricle visible when moving (Fig. 7a). Proventricle prominent, barrel-shaped, almost as wide as body width, filling coelomic cavity, extending through 4–5 segments (15–18 in holotype) (Figs. 5a and 7a). Alimentary canal continuous through all branches. Content visible by transparency as a transparent fluid (Fig. 8a), occasionally with some brownish particles (Fig. 8c). No sponge tissue identified inside. Content of digestive tube moving through peristalsis in vivo, with posterior ends (last 10–20 segments, including anus) internally densely covered by cilia (Video S2) visible by transparency and through anus (Fig. 10c, d). A pair of nephridia per segment at basis of parapodia (Video S3). Each branch with a wide ventral blood vessel visible by transparency (Fig. 8h), ventral to, and wider than digestive tube (Fig. 8i), with a transparent fluid circulating inside and showing peristalsis (Video S4). Incomplete intersegmental anterior and posterior septa delimitate each segment. Digestive tube and ventral blood vessel slightly thinner when going through intersegmental septa (Fig. 8h). Nerve cord ventral, with multiple ramifications (Fig. 13a). Body wall muscles longitudinal, circular ones not seen. External body bifurcation

at branching points accompanied by bifurcation of all longitudinal organs (ventral nerve cord, longitudinal muscles, digestive tube, and ventral blood vessel) (Figs. 13a, b), which occupy same relative position in new branches. "Muscular bridge" crossing dorsally over intestine and between ventral nerve cord and ventral blood vessel ventrally to one of three segments coming out from branching point (Fig. 13a, b), being delimited by three Y-shaped intersegmental septa (Fig. 11h, i; Video S3).

Reproduction and regeneration Sexes separate. Reproduction by gemmiparous schizogamy. Numerous stolons of same sex at end of terminal branches. Attached and detached stolons in a given host sponge are consistently of single sex (either male or female). Stalks undistinguishable from internodes (areas between two branching points) and other terminal branches lacking signs of gametogenesis (Fig. 14i). Segments from stalk with clear alternation in dorsal cirri length (Fig. 14i). No correlation between number of stalk segments and stolon maturity. Ventral regeneration of stalk pygidium starting before stolon detachment (Figs. 13h and 14g, h). Stalks with recently detached stolons showing stubby endings, still ventrally directed, with signs of stolon attachment dorsally, clearly differing from growing tips of new stolons or of developing branches (Figs. 8b, g, and 13f). When dorsal surfaces are repaired, a pair of anal cirri and a new anal opening are developed, followed by regular growth and addition of segments just in front of newly formed pygidium (Fig. 12).

Stolons acerous, with bilobed anterior end, lacking antennae and palps (Figs. 13c, d, and 14a–f). Two pairs of well-developed dorsal (posterior) and ventral (anterior) eyes; ventral pair larger than dorsal one (Fig. 14g, h). A vestigial digestive tube through males and female's stolon segments, bubble like in female first segments, very narrow in remaining segments. Mature female and male stolons having dense bundles of long paddle-like natatory chaetae in addition to typical stock neurochaetae, transparent, long, distally pointed ("wing- or leaf-like") (Fig. 13e), developing in mature stolons, usually seen in recently detached ones. Not seen in still attached, non-fully developed stolons.

Male stolons similar in size to female stolons, but with considerably longer parapodia and narrower bodies (Figs. 13c and 14f), with first two pairs of dorsal cirri longer than following ones (Fig. 14f) and internal oval structures at basis of parapodia (Fig. 13i) (possibly chaetal sacs of the paddle-like chaetae), with first three segments full of yellowish sperm (regionalization) (Fig. 14f). Female stolons with marked positive phototaxis when mature and detached (Video S5), all dorsal cirri of about same length, and segments full of oocytes, even in parapodia (Fig. 14a–e), pink in detached females, white in not completely developed females (Fig. 14c–e). Developing larvae or embryos not observed.
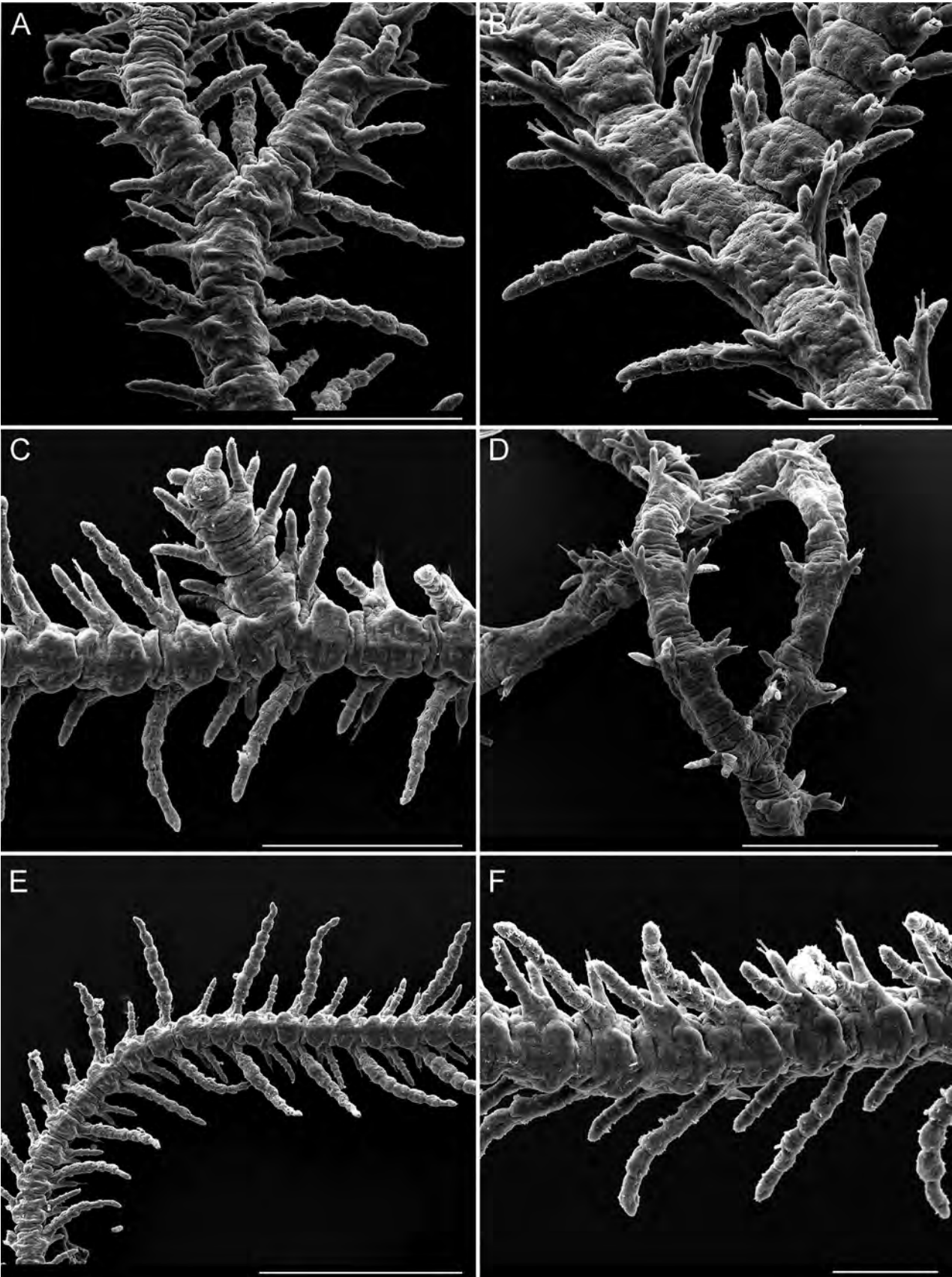
◄**Fig. 9** Scanning electron microscopy images of branches of *Ramisyllis kingghidorahi* n. sp. **A–F** Midbody branching regions with segments of different morphologies, as long as wide with long dorsal cirri in **A–C**, much longer with short dorsal cirri in **D**, **E** and **F** Details of cirri alternation in length. **A**, **C**, **E–F** In dorsal view; **B** and **D** in ventral view. Scale bars: 200 μm **A**, **C**, 100 μm **B**, **F**, 400 μm **D**, and 500 μm **E**

Remarks *Ramisyllis kingghidorahi* n. sp. and *R. multicaudata* (Glasby et al., 2012; Ponz-Segrelles et al., 2021; Schroeder et al., 2017) differ from *S. ramosa* (except the Red Sea and Imajima's 2005 Sagami Bay specimens) in living from 0 to 20-m depth inside species of *Petrosia* instead of 100–1000 m depth inside species of *Crateromorpha* (Izuka, 1912; McIntosh, 1879; Oka, 1895); in having the proliferating area after the parapodia and never replacing it or the dorsal cirri (Glasby et al., 2012) instead of new branches emerging from the parapodium and lacking dorsal cirri as in *S. ramosa*; in lacking two branches emerging from both sides of the same segment, which may occur in *S. ramosa* (Pl. XXIII, Fig. 11 in McIntosh,; Fig. 2 in Oka, 1895); in having simple, robust, tomahawk-shaped chaetae instead of slender, hooked at the tip and a fusion line between shaft and blade in *S. ramosa* (Pl. XVIA; Fig. 1 in McIntosh, 1885); and in newly formed branches acquiring very soon the segment size and cirri length of previous branches instead of showing differences in segments width and smaller and shorter than usual dorsal cirri in *S. ramosa* (e.g., Fig. 18 in Okada (1937)).

Ramisyllis kingghidorahi n. sp. lives inside an undescribed *Petrosia* sponge and *R. multicaudata* in another unidentified species of *Petrosia* (probably *Petrosia* cf. *nigricans*, pers. comm. Dirk Erpenbeck), in both clearly different ecosystems (costal coral reef *vs.* rubble sand with algae, respectively) at different latitudes with different water temperatures. Dorsal cirri are generally longer in *R. kingghidorahi* n. sp. than in *R. multicaudata*, particularly in the anterior end (Fig. 7a, b; Online Resource 11), the proventricle is also longer (4–5 *vs.* 2–4 segments) (Online Resource 11), stalks are similar to segments in regular branches, while these are narrower with shorter dorsal cirri in *R. multicaudata* (as in *S. ramosa*) and their stolons also slightly differ in the relative length of some features (e.g., dorsal and ventral cirri, Online Resource 12). In *R. kingghidorahi* n. sp. the development of a new branch seems to occur just in the intersegmental area, while it was described that in *R. multicaudata*, it begins in front of the posterior septum (Glasby et al., 2012). In *R. kingghidorahi* n. sp. intersegmental septa of the two pre-existing segments and the newly formed one can be observed by transparency (Fig. 11h, i); they form a "Y" shape (Fig. 11h, i,; Video S3), and appeared to be reduced as in *R. multicaudata* (Ponz-Segrelles et al., 2021), allowing the thinner digestive tube and ventral blood

vessel to pass through them (Fig. 8h, i). Nevertheless, in both species, all longitudinal organs bifurcate in the branching points, new branches show internal muscular bridges crossing between the different organs and the ventral blood vessel is considerably enlarged in comparison with other syllids and similar in diameter to the digestive tube (Ponz-Segrelles et al., 2021).

The three branching syllids show segmental asymmetry (i.e., segments with pairs of dorsal cirri of different length on each side), which intervenes between regions of symmetry (Schroeder et al., 2017) and have been found to show reddish coloration (Glasby et al., 2012; Imajima, 1966; Read, 2001). The glandular material of dorsal cirri in *R. multicaudata* changes from bright white into red colour when the animals start dying (Ponz-Segrelles et al., 2021), and we observed a similar phenomenon in *R. kingghidorahi* n. sp., with this material protruding through the dorsal cirri pores.

The precise behaviour of female stolons once detached was not determined in *R. multicaudata*, although the presence of paddle chaetae suggested enhanced swimming ability (Ponz-Segrelles et al., 2021; Schroeder et al., 2017). In *R. kingghidorahi* n. sp., female stolons showed a clear positive phototaxis (Video S5) which, together with the paddle-like natatory chaetae, suggests that they leave the sponges for spawning. *Syllis ramosa* from the Philippines type locality might be viviparous (McIntosh, 1885), but this was neither confirmed for the type material by Glasby et al. (2012), nor for the two species of *Ramisyllis.*

Previous reports of *S. ramosa* could represent more than one branching species (Glasby et al., 2012), including, for instance, the Red Sea specimen inhabiting a shallow water silicious sponge. Indeed, in agreement with Leslie Harris (pers. comm.), we suggest that a picture by Danièle Heitz of a *Petrosia* from the Red Sea (Al Birk) with syllid branches emerging from one osculum (https://nomadica.jimdofree.com/vers-marins/annélides/ramisyllis-multicaudata/) likely corresponds to an undescribed species of *Ramisyllis*. The specimen from Sagami Bay identified by Imajima in 2005 shows differences in chaetal morphology, compared with the three currently known branching species and, thus, might also be an undescribed species. The report of *S. ramosa* from the southern coast of Jeju Island in South Korea (Lee, 1992) is herein considered as dubious, since it was found on mollusc shells and had compound chaetae.

Discussion

Ramisyllis kingghidorahi, a new branching species

All our biological and ecological observations, morphological analyses, internal anatomy observations, and phylogenetic and genetic distance analyses consistently support
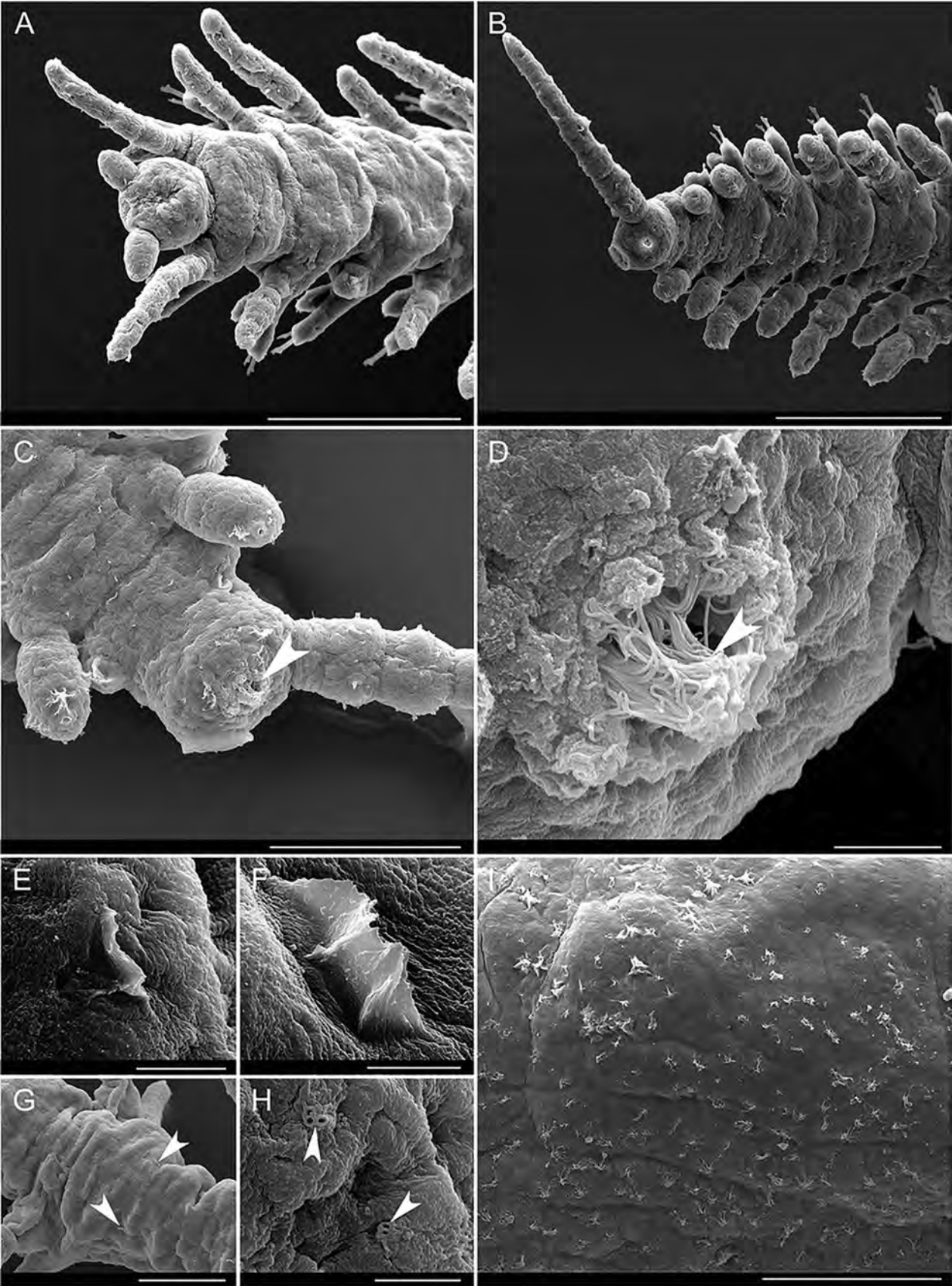
recognition of *R. kingghidorahi* n. sp. as a new species, closely related to *R. multicaudata*. The morphological differences, though clear and consistent among studied specimens, are subtle, and might not be easy to detect by a non-expert eye. This morphological semi-stasis between two clear phylogeographic lineages might be explained by a strict conserved niche (Cerca et al., 2020, 2021) like the *Petrosia* canal system in which these animals live.

The asymmetrical branching body with unpaired branching may have been inherited from the last common ancestor of both species of *Ramisyllis*, which was probably already adapted to live inside a sponge canal system. Including *S. ramosa* in a phylogenetic analysis has not been possible. Hence, the reconstruction of ancestral features must consider two possible scenarios: (1) *S. ramosa* joining *R. multicaudata* and *R. kingghidorahi* in a monophyletic group and (2) *S. ramosa* not being sister to *R. multicaudata* and *R. kingghidorahi*. Under the second scenario, all observed morphological similarities would need to be understood as convergencies resulting from independent adaptations likely related to life in symbiosis with sponges.

Phylogenetic topologies reveal sister group relationships between both species of *Ramisyllis*, with a clear divergence in *COI* and *16S* (which show faster mutations rates than the nuclear *18S* and *28S*). The very high *COI* distances between both species of *Ramisyllis* agree with previous studies delimitating species in syllids and annelids in general (Aguado et al., 2019; Álvarez-Campos et al., 2017; Kvist, 2016; Lobo et al., 2016; Nygren et al., 2018), as well as those found for the *16S* (Bastrop et al., 1998; Gunton et al., 2020; Miglietta et al., 2010; Radashevsky et al., 2016) and *ITS2* markers (Vivien et al., 2015). Conversely, the *28S* distance was 1 order of magnitude lower but still significant since this is a slow evolving gene and the obtained distances were similar to those among other syllids (Aguado et al., 2019). In *18S* (also a slow evolving gene), distances were lower still. The conserved nuclear gene *18S* has previously been used in annelid species delimitation studies as a phylogenetic marker (Cerca et al., 2020, 2021) but is known to usually underestimate the number of species (Tang et al., 2012). Interestingly, *Ramisyllis* species highly differ from the other syllids in their *18S* sequences as revealed by the long branch in the phylogenetic analysis (Fig. 2a) and the clear differences in *18S* alignments (Aguado et al., 2015a). This is probably due to expansion regions particularly

variable in syllids (Aguado & Bleidorn, 2010), though its significance is still unknown. The *28S* branch is also quite long, although the comparison in this case is less meaningful due to the lower number and quality of the available sequences of Syllinae.

The mt-genome of *R. kingghidorahi* n. sp. resembles that of *R. multicaudata* in gene order, AT and GC skews, codon usage bias, and secondary structure of most tRNAs (Aguado et al., 2015a). However, it strongly differs from most available syllid mt-genomes (Aguado et al., 2016, 2015a), particularly in having a strongly modified gene order and highly derived nuclear ribosomal sequences.

The evolutionary meaning of a branching body

Many annelids (including syllids) grow by adding segments in front of the pygidium from a segment addition zone (SAZ) (Balavoine, 2014; Bely, 2006; Zattara & Weisblat, 2020). In *Ramisyllis*, this occurs simultaneously at the multiple SAZs before each pygidium, more than 500 in *R. multicaudata* (Glasby et al., 2012). The branching ability is related to the presence of multiple SAZs and, thus, it allows these animals to reach a huge size compared with other syllids (usually measuring some mm to few cm). *R. multicaudata* may reach 30 m long by considering all branches linearly placed one after another (GPS & MTA, pers. obs.).

The "muscular bridges" at the branching points found in *R. multicaudata* (Ponz-Segrelles et al., 2021) also occur in *R. kingghidorahi* (Fig. 13a, b). This feature reveals that the bifurcation process does not occur in the SAZ in front of the pygidium, but laterally from fully-developed, mid-body segments. Consequently, the genetic growth-controlling mechanisms usually expressed in the posterior end (Ponz-Segrelles et al., 2018) have to be active in mid-body segments or, alternatively these species may have developed new growth-control mechanisms.

The concatenated topology (Fig. 3) shows the *Ramisyllis* clade as sister to a group comprising *Trypanobia* and *Trypanedenta*, as in Aguado and et al. (2015a), with *Trypanedenta gemmipara*, *Trypanedenta gigantea*, and *Trypanobia depressa* (Augener, 1913) reproducing by gemmiparity. *Trypanedenta gigantea* shows serial gemmiparity (sensu Aguado et al., 2015a), thus producing stolon chains (Álvarez-Campos et al., 2018). *Trypanedenta gemmipara* shows collateral gemmiparity (sensu Aguado et al., 2015a), thus producing a bunch of stolons attached to a proliferating area in front of the pygidium (Johnson, 1902). *Trypanedenta asterobia* shows successive gemmiparity (sensu Aguado et al., 2015a), thus developing stolons in various consecutive posterior segments. This is particularly interesting since stolons are formed not only near the pygidium SAZ, but also in several posterior segments (Okada, 1933, 1937), which may imply a simultaneous activation of genetic machinery
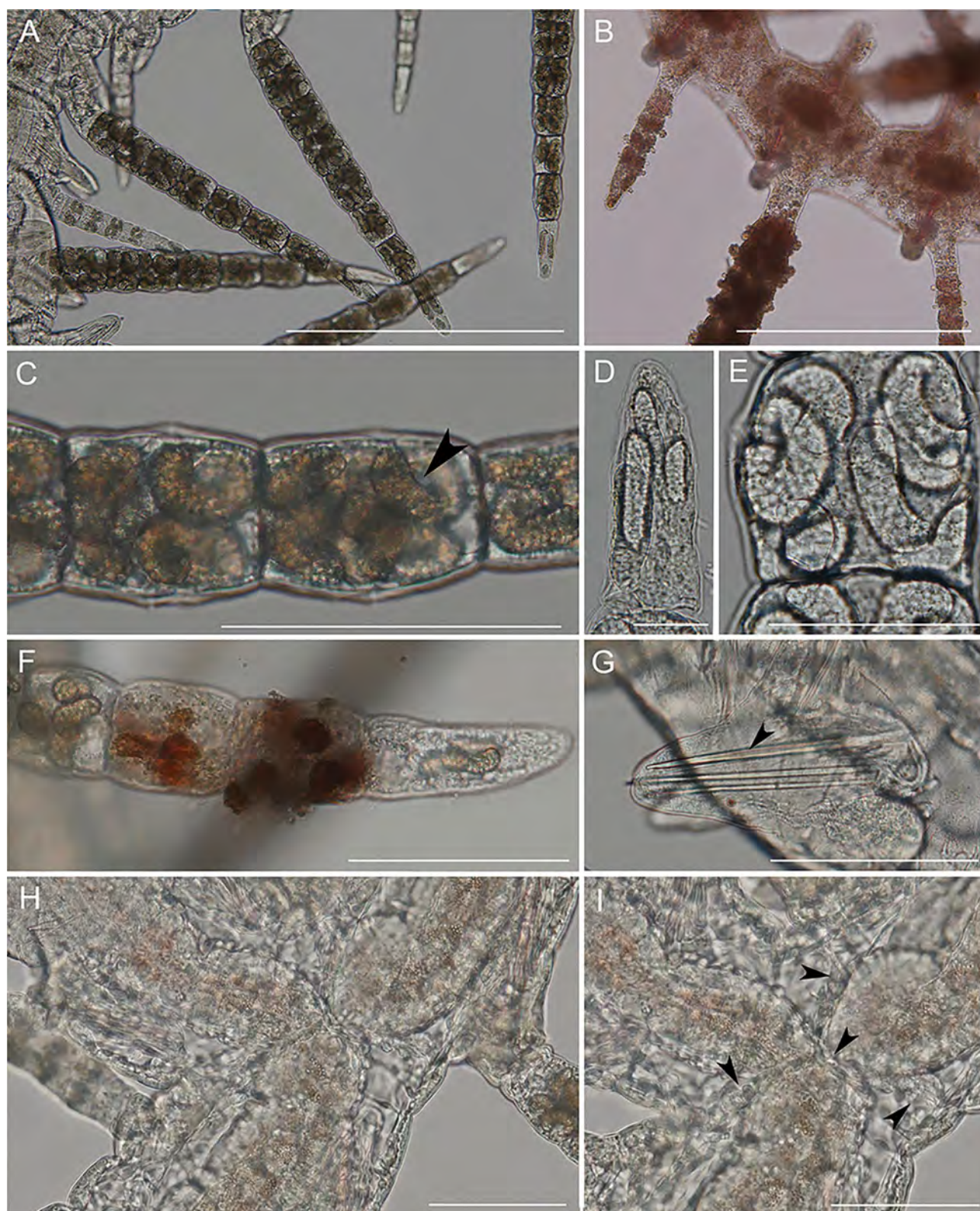
Fig. 11 Light microscope images of living specimens of *Ramisyllis kingghidorahi* n. sp., dorsal cirri, parapodium and segmental septa. **A–F** Dorsal cirri and spiral glands; arrow points to spiral gland in **C**. **G** Midbody parapodium, arrow points to pointed acicula, lateral view. **H–I** Three intersegmental septa forming a "Y shape," dorsal view. Scale bars: 200 μm **A**, **B**, 50 μm **C**, **F**, **G**, **H**, **I**, 20 μm **E**, and 10 μm **D**
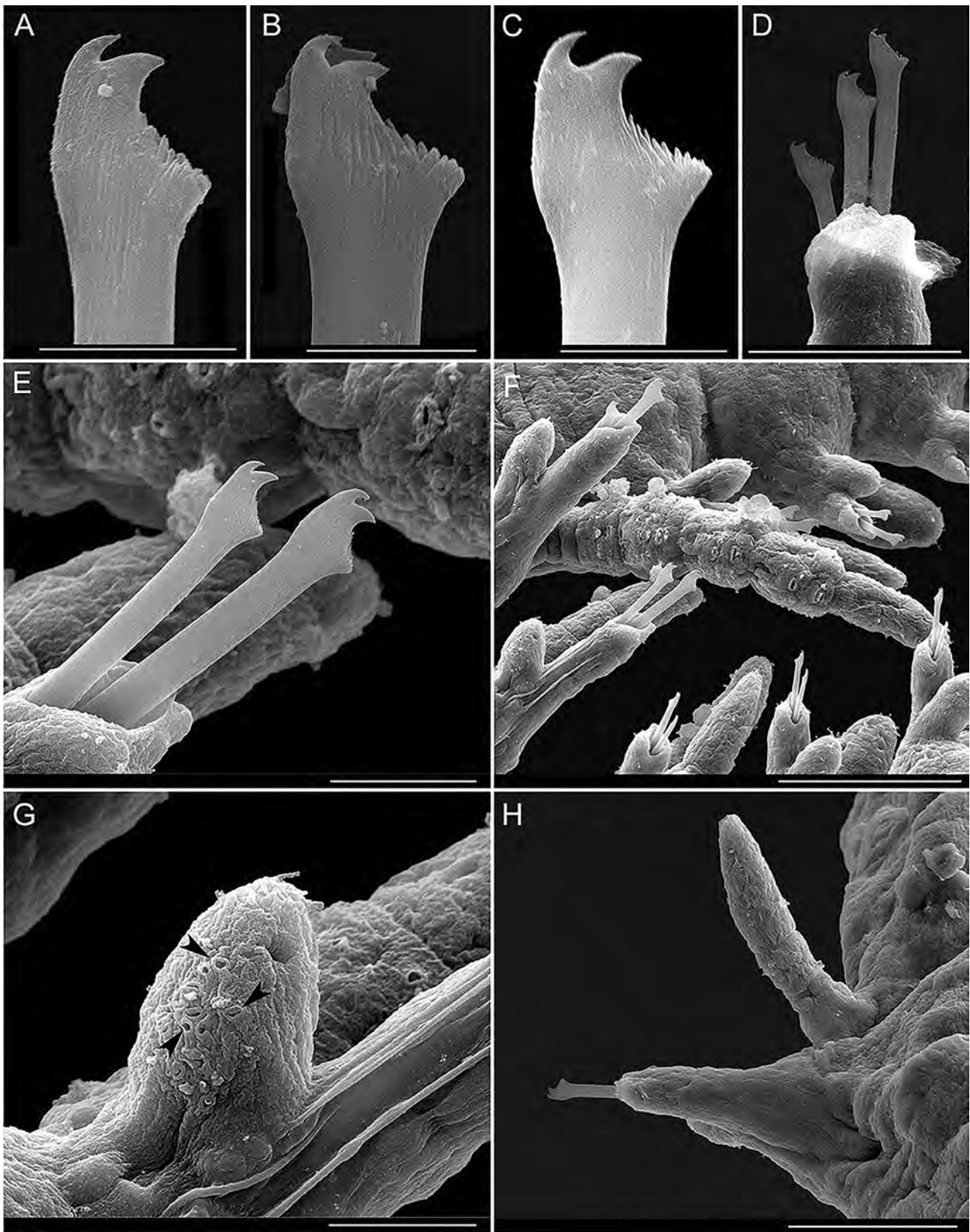
Fig. 12 Scanning microscopy images of *Ramisyllis kingghidorahi* n. sp, parapodium and chaetae details. **A–F**, **H** Midbody tomahawk shaped chaetae. **G** Ventral cirri, arrows point to pores. Scale bars: 5 μm **A**, **C** 4 μm **B**, 20 μm **D**, 10 μm **E**, **G**, and 50 μm **F**, **H**
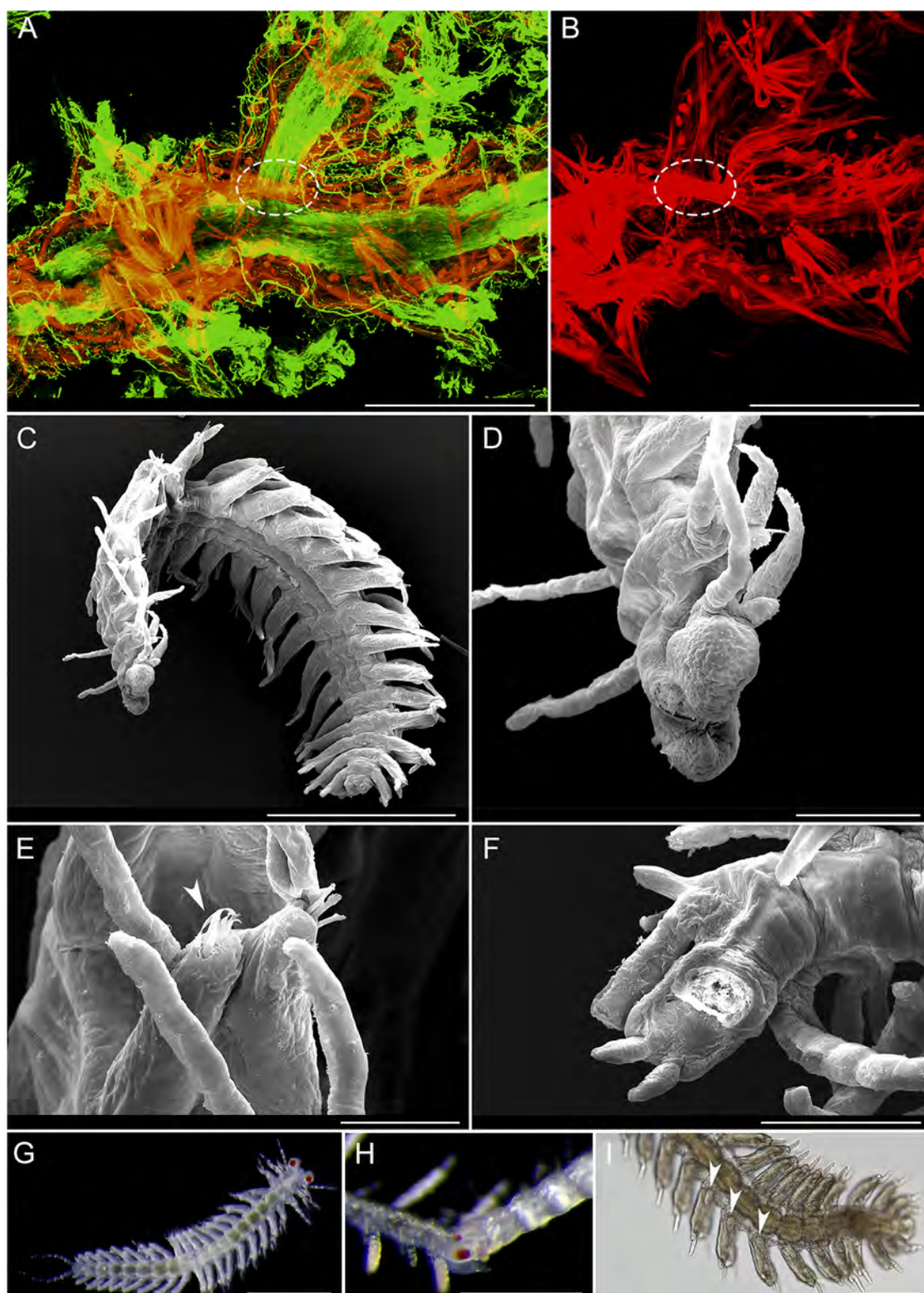
Fig. 13 Internal anatomical details of a branch and scanning microscopy images of stolons. **A**, **B** cLSM images of musculature and nervous system immunohistochemical stainings at a branching point, dashed-lined circles mark muscle bridges. **C** Male stolon. **D** Head of a male stolon. **E** Stolon parapodium, arrow points to paddle-like modified chaetae. **F** Regenerating pygidium, after detachment of stolon. **G** Male stolon detached. **H** Stolon attached to the stalk segments. **I** Posterior segments of male stolon, ventral view, arrows point to oval structures, at the base of parapodia. Scale bars: 250 μm **A**, **B**, **H**, **I**, 500 μm **C**, **G**, 100 μm **D**, **F**, and 50 μm **E**
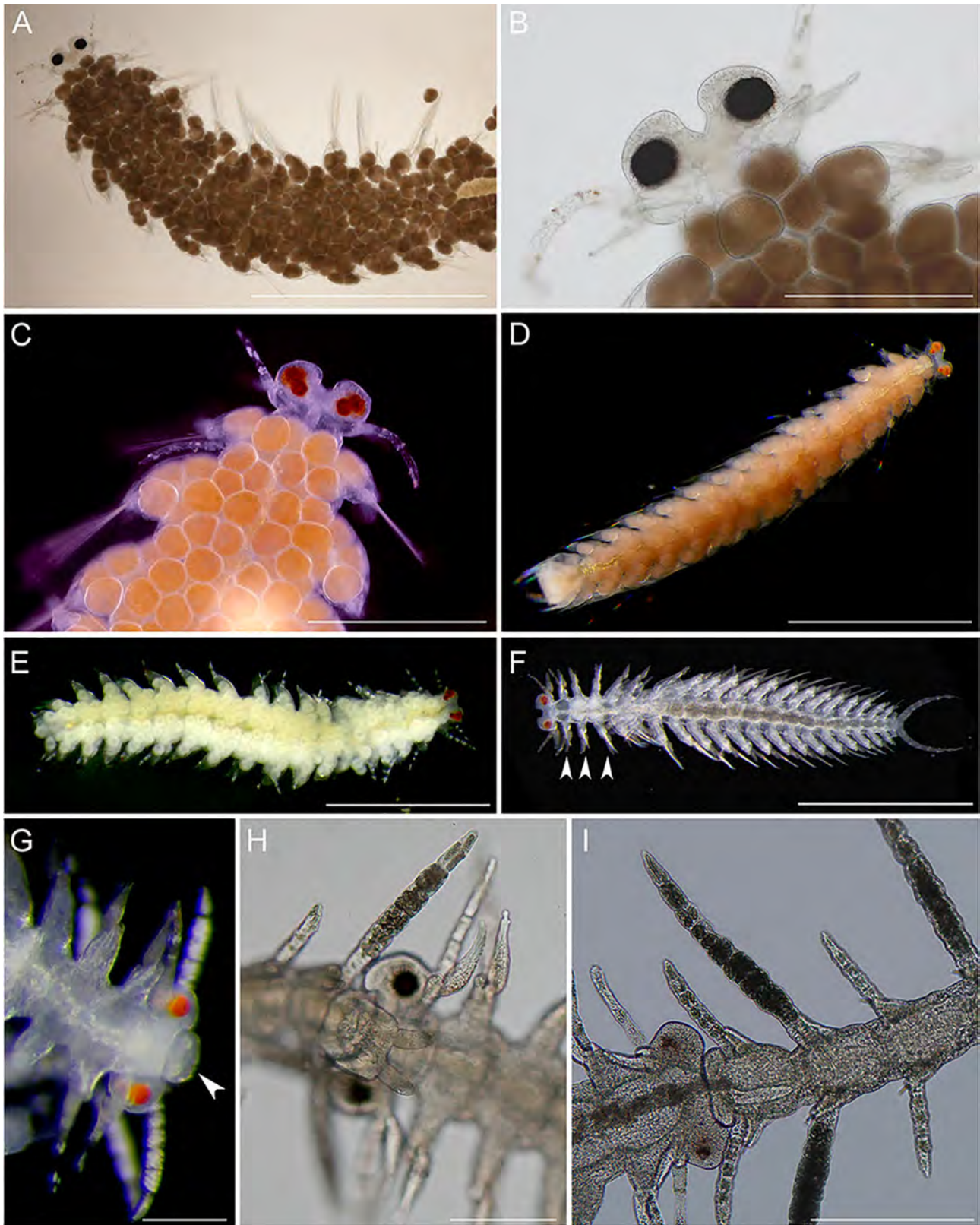
Fig. 14 Sexual dimorphism in stolons. **A–E** Female stolons, dorsal view. **F–I** Male stolons; arrows in **F** point to the first three segments, the only ones that contain sperm. **G–I** Stolons attached to the stalk, detail of pygidium in regeneration on the ventral side before detachment of the stolon (arrow in **G**), ventral view. **H** Light microscope image showing region of stolon head and pygidium regeneration, ventral view. **I** Stolon attached, dorsal view. Scale bars: 500 μm **A**, **D**, **E**, **F**, 100 μm **B**, **G**, **H**, and 200 μm **C**, **I**

and regulation processes controlling the development of new tissues in different segments in a way similar to branching syllids (Aguado et al., 2015a). Another species of *Trypanobia*, *T. cryptica*, was described with only one non fully developed stolon (Aguado et al., 2015b). Thus, it is not clear if it would be able to develop more. Accordingly, the concatenated topology (Fig. 3) reveals the presence of gemmiparity in the common ancestor of *Trypanedenta-Trypanobia* and *Ramisyllis* as being the most parsimonious reconstruction. In addition, several *Trypanobia* species are known to maintain symbiotic relationships with other organisms, such as starfishes and sponges (Aguado et al., 2015b; Okada, 1933), so its hypothetical ancestor might have also been a symbiont.

Symbiotic relationships are frequent in syllids (Martin & Britayev, 1998, 2018). For instance, species of *Haplosyllides* Augener, 1922 and *Haplosyllis* Langerhans, 1879 also live inside sponge canals (Martin et al., 2003, 2009), though they may have developed a different mechanism to infest their sponge hosts. Instead of branching, they have evolved into minute bodies but may reach enormous densities inside the hosts (Martin & Britayev, 2018), which, to some extent, mimics the branching strategy. Aguado and et al. (2015a) showed that *Ramisyllis* is not closely related to *Haplosyllis*, the latter being a member of the large and taxonomically complex Clade B (sensu Ribeiro et al., 2020). However, *Haplosyllides* has never been included in a previous molecular phylogenetic analysis and a closer relationship with the branched syllids cannot be ruled out. *Haplosyllis* species have been demonstrated to feed on sponge tissues, likely taking profit of the sponge symbiotic bacteria rather than on the sponge cells (Turon et al., 2019). Aguado and et al. (2015a) did not find any trace of the sponge contamination in the genome data of *R. multicaudata*, which together with no visual evidence of sponge tissue in the digestive tube of *Ramisyllis* may indicate that branching species do not feed on their host sponges. However, further studies involving more specific techniques, e.g., stable isotope and fatty acids analyses (Taboada et al., 2021) and sponge and worm microbiomes characterization (Turon et al., 2019), would be necessary for more conclusive results. The finding of highly ciliated digestive tubes, especially at the posterior ends and ani, might indicate the use of posterior ends for incorporating fluids into the digestive system. The incorporation of water and food through the posterior end (anus) instead of, or in addition to, the anterior one (mouth) has been reported before in other animals such as holothurians (Jaeckle & Strathmann, 2013). An uptake of ambient water and certain nutrients through the anus has been also proposed as a possible osmotic balance mechanism for some annelids (Jumars et al., 2015). However, more investigations are needed to confirm this hypothesis.

The acquisition of a complex multiaxial body may be related with an increasing reproductive success, as having multiple posterior ends allows the simultaneous production of numerous stolons at the same time. This ability might sustain the apparently small populations found for *R. multicaudata* and *R. kingghidorahi* n. sp. However, this ability might also be considered a consequence of having a multibranched body. In any case, such a complex body may only be explained by considering the sponge and the worm as a holobiont (Turon et al., 2019). The ramified bodies of the branching syllids might mirror the intricate labyrinth of the sponge canal system in which they live, the sponge canal system, with the ability to produce new fully-developed segments allowing the worm to explore the canals. As such, this can be understood as an example of a change of habitat (from free-living in soft or hard bottoms to inhabiting sponge canals) allowing for the emergence of an evolutionary novelty (branching body) by modification of existing developmental biases which prevented or limited variation (Holló & Novák, 2012) and, consequently, setting the stage for the evolution of a symbiotic relationship.

Declarations

Ethical approval Not applicable.

Consent to participate Not applicable.

Consent for publication Not applicable.

Conflict of interest The authors declare no competing interests.

References

Agassiz, A. (1862). On alternate generation of annelids and the embryology of *Autolytus cornutus*. *Boston Journal of Natural History, 7*(3), 384–409.

Aguado, M. T., & Bleidorn, C. (2010). Conflicting signal within a single gene confounds syllid phylogeny (Syllidae, Annelida). *Molecular Phylogenetics and Evolution, 55*(3), 1128–1138. https://doi.org/10.1016/j.ympev.2010.01.012

Aguado, M. T., Capa, M., Lago-Barcia, D., Gil, J., Pleijel, F., & Nygren, A. (2019). Species delimitation in *Amblyosyllis* (Annelida, Syllidae). *PLoS ONE, 14*(4), e0214211. https://doi.org/10.1371/journal.pone.0214211

Aguado, M. T., Glasby, C. J., Schroeder, P. C., Weigert, A., & Bleidorn, C. (2015a). The making of a branching annelid: An analysis of complete mitochondrial genome and ribosomal data of *Ramisyllis multicaudata*. *Scientific Reports, 5*, 12072. https://doi.org/10.1038/srep12072

Aguado, M. T., Murray, A., & Hutchings, P. (2015b). Syllidae (Annelida: Phyllodocida) from Lizard Island, Great Barrier Reef, Australia. *Zootaxa*, *4019*(1), 035–060. https://doi.org/10.11646/zootaxa.4019.1.5

Aguado, M. T., Richter, S., Sontowski, R., Golombek, A., Struck, T. H., & Bleidorn, C. (2016). Syllidae mitochondrial gene order is unusually variable for Annelida. *Gene, 594*(1), 89–96. https://doi.org/10.1016/j.gene.2016.08.050

Aguado, M. T., San Martín, G., & Siddall, M. E. (2012). Systematics and evolution of syllids (Annelida, Syllidae). *Cladistics, 28*, 234–250. https://doi.org/10.1111/j.1096-0031.2011.00377.x

Altschul, S. F., Gish, W., Miller, W., Myers, E. W., & Lipman, D. J. (1990). Basic local alignment search. *Journal of Molecular Biology, 215*, 403–410. https://doi.org/10.1016/S0022-2836(05)80360-2

Álvarez-Campos, P., Giribet, G., & Riesgo, A. (2017). The *Syllis gracilis* species complex: A molecular approach to a difficult taxonomic problem (Annelida, Syllidae). *Molecular Phylogenetics and Evolution, 109*, 138–150. https://doi.org/10.1016/j.ympev.2016.12.036

Álvarez-Campos, P., Taboada, S., San Martín, G., Leiva, C., & Riesgo, A. (2018). Phylogenetic relationships and evolution of reproductive modes within flattened syllids (Annelida, Syllidae) with the description of a new genus and six new species. *Invertebrate Systematics, 32*, 224–251. https://doi.org/10.1071/IS17011

Augener, H. (1913). Polychaeta I, Errantia. In W. Michaelsen & R. Hartmeyer (Eds.), *Die Fauna Südwest-Australiens. Ergebnisse der Hamburger südwest-australischen Forschungsreise, 1905* (Vol. 4, Issue 5, pp. 65–305). Gustav Fischer. https://doi.org/10.1038/077051b0

Augener, H. (1922). Ueber litorale Polychaeten von Westindien. *Sitzungsberichte Der Gesellschaft Naturforschende Freunde Zur Berlin, 3–5*, 38–53.

Balavoine, G. (2014). Segment formation in Annelids: Patterns, processes and evolution. *International Journal of Developmental Biology, 58*, 469–483. https://doi.org/10.1387/ijdb.140148gb

Bastrop, R., Jürss, K., & Sturmbauer, C. (1998). Cryptic species in a marine polychaete and their independent introduction from North America to Europe. *Molecular Biology and Evolution, 15*(2), 97–103. https://doi.org/10.1093/oxfordjournals.molbev.a025919

Bely, A. E. (2006). Distribution of segment regeneration ability in the Annelida. *Integrative and Comparative Biology, 46*(4), 508–518. https://doi.org/10.1093/icb/icj051

Bernt, M., Donath, A., Jühling, F., Externbrink, F., Florentz, C., Fritzsch, G., Pütz, J., Middendorf, M., & Stadler, P. F. (2012). MITOS: Improved de novo metazoan mitochondrial genome annotation. *Molecular Phylogenetics and Evolution, 69*(2), 313–319. https://doi.org/10.1016/j.ympev.2012.08.023

Bolger, A. M., Lohse, M., & Usadel, B. (2014). Trimmomatic: A flexible trimmer for Illumina sequence data. *Bioinformatics, 30*(15), 2114–2120. https://doi.org/10.1093/bioinformatics/btu170

Castresana, J. (2000). Selection of conserved blocks from multiple alignments for their use in phylogenetic analysis. *Molecular Biology and Evolution, 17*(4), 540–552. https://doi.org/10.1093/oxfordjournals.molbev.a026334

Cerca, J., Colon, A. G. R., Ferreira, M. S., Ravinet, M., Nowak, M. D., Catchen, J. M., & Struck, T. H. (2021). Incomplete lineage sorting and ancient admixture, and speciation without morphological change in ghost-worm cryptic species. *PeerJ, 9*, e10896. https://doi.org/10.7717/peerj.10896

Cerca, J., Meyer, C., Stateczny, D., Siemon, D., Wegbrod, J., Purschke, G., Dimitrov, D., & Struck, T. H. (2020). Deceleration of morphological evolution in a cryptic species complex and its link to paleontological stasis. *Evolution, 74*(1), 116–131. https://doi.org/10.1111/evo.13884

Chernomor, O., Von Haeseler, A., & Minh, B. Q. (2016). Terrace aware data structure for phylogenomic inference from supermatrices. *Systematic Biology, 65*(6), 997–1008. https://doi.org/10.1093/sysbio/syw037

Conant, G. C., & Wolfe, K. H. (2008). GenomeVx: Simple web-based creation of editable circular chromosome maps. *Bioinformatics, 24*(6), 861–862. https://doi.org/10.1093/bioinformatics/btm598

Crossland, C. (1933). Distribution of the polychaete worm, *Syllis ramosa*, McIntosh. *Nature*, *31*, 242 (only). https://doi.org/10.1038/131242a0

Folmer, O., Black, M., Hoeh, W., Lutz, R., & Vrijenhoek, R. (1994). DNA primers for amplification of mitochondrial cytochrome c oxidase subunit I from diverse metazoan invertebrates. *Molecular Marine Biology and Biotechnology, 3*(5), 294–299. https://doi.org/10.1371/journal.pone.0013102

Forsskål, P. (1775). *Descriptiones animalium, avium, amphibiorum, piscium, insectorum, vermium; quae in itinere orientali observavit Petrus Forskål. Post mortem auctoris edidit Carsten Niebuhr*. Ex officina Mölleri.

Franke, H.-D. (1999). Reproduction of the Syllidae (Annelida: Polychaeta). *Hydrobiologia, 402*(2), 39–55. https://doi.org/10.1023/A:1003732307286

Glasby, C. J., Schroeder, P. C., & Aguado, M. T. (2012). Branching out: A remarkable new branching syllid (Annelida) living in a *Petrosia* sponge (Porifera: Demospongiae). *Zoological Journal*

of the Linnean Society, 164, 481–497. https://doi.org/10.1111/j.1096-3642.2011.00800.x

Grabherr, M. G., Haas, B. J., Yassour, M., Levin, J. Z., Thompson, D., & a, Amit, I., Adiconis, X., Fan, L., Raychowdhury, R., Zeng, Q., Chen, Z., Mauceli, E., Hacohen, N., Gnirke, A., Rhind, N., di Palma, F., Birren, B. W., Nusbaum, C., Lindblad-Toh, K., … Regev, A. (2011). Full-length transcriptome assembly from RNA-Seq data without a reference genome. *Nature Biotechnology, 29*(7), 644–652. https://doi.org/10.1038/nbt.1883

Gray, J. E. (1872). On a new genus of hexaradiate and other sponges discovered in the Philippine Islands by Dr. A.B. Meyer. *Annals and Magazine of Natural History Series IV, 10*(56), 134–139. https://doi.org/10.1080/00222937208696659

Grube, A. E. (1863). Beschreibung neuer oder wenig bekannter Anneliden. *Sechster Beitrag. Archiv Für Naturgeschichte, 29*, 37–69. https://doi.org/10.5962/BHL.PART.9306

Gunton, L. M., Kupriyanova, E., & Alvestad, T. (2020). Two new deep-water species of Ampharetidae (Annelida: Polychaeta) from the eastern australian continental margin. *Records of the Australian Museum, 72*(4), 101–121. https://doi.org/10.3853/J.2201-4349.72.2020.1763

Gurevich, A., Saveliev, V., Vyahhi, N., & Tesler, G. (2013). QUAST: Quality assessment tool for genome assemblies. *Bioinformatics, 29*(8), 1072–1075. https://doi.org/10.1093/bioinformatics/btt086

Haas, B. J., Papanicolaou, A., Yassour, M., Grabherr, M., Philip, D., Bowden, J., Couger, M. B., Eccles, D., Li, B., Macmanes, M. D., Ott, M., Orvis, J., & Pochet, N. (2013). De novo transcript sequence reconstruction from RNA-seq using the Trinity platform for reference generation and analysis. *Nature Protocols, 8*(8), 1–43. https://doi.org/10.1038/nprot.2013.084

Hall, T. A. (1999). BioEdit: A user-friendly biological sequence alignment editor and analysis program for Windows 95/98/NT. *Nucleic Acids Symposium Series, 41*, 95–98.

Hartmann-Schröder, G. (1962). Die Polychaeten des Eulitorals. In: Hartmann-Schröder, G. and Gerd Hartmann. Zur Kenntnis des Eulitorals der chilenischen Pazifikküste und der argentinischen Küste Südpatagoniens unter besonderer Berücksichtigung der Polychaeten und Ostracoden. *Mitteilungen Aus Dem Hamburgischen Zoologischen Museum Und Institut, 60*, 57–270.

Holló, G., & Novák, M. (2012). The manoeuvrability hypothesis to explain the maintenance of bilateral symmetry in animal evolution. *Biology Direct, 7*(22), 1–7. https://doi.org/10.1186/1745-6150-7-22

Ijima, I. (1898). The genera and species of Rosselidae. *Annotationes Zoologicae Japonenses, 2*(3), 41–55.

Imajima, M. (1966). The Syllidae (polychaetous annelids) from Japan (IV) syllinae (1). *Publications of the Seto Marine Biological Laboratory, 14*(3), 219–252. https://doi.org/10.5134/175436

Izuka, A. (1912). The errantiate Polychaeta of Japan. *Journal of the College of Science, Imperial University of Tokyo, 30*(2), 1–262. https://doi.org/10.1126/science.ns-18.446.109

Jaeckle, W. B., & Strathmann, R. R. (2013). The anus as a second mouth: Anal suspension feeding by an oral deposit-feeding sea cucumber. *Invertebrate Biology, 132*(1), 62–68. https://doi.org/10.1111/ivb.12009

Johnson, H. P. (1901). The Polychaeta of the Puget Sound region. *Proceedings of the Boston Society for Natural History, 29*(18), 381–437.

Johnson, H. P. (1902). Collateral budding in annelids of the genus *Trypanosyllis*. *The American Naturalist, 36*(424), 295–315. https://doi.org/10.1086/278120

Jumars, P. A., Dorgan, K. M., & Lindsay, S. M. (2015). Diet of worms emended: An update of polychaete feeding guilds. *Annual Review of Marine Science, 7*, 497–520. https://doi.org/10.1146/annurev-marine-010814-020007

Kalyaanamoorthy, S., Minh, B. Q., Wong, T. K. F., Haeseler, A. Von, & Jermiin, L. S. (2017). ModelFinder: Fast model selection for accurate phylogenetic estimates. *Nature Methods, 14*, pages587–589. https://doi.org/10.1038/nmeth.4285

Katoh, K., Rozewicki, J., & Yamada, K. D. (2017). MAFFT online service: Multiple sequence alignment, interactive sequence choice and visualization. *Briefings in Bioinformatics, 20*(4), 1160–1166. https://doi.org/10.1093/bib/bbx108

Katoh, K., & Standley, D. M. (2013). MAFFT multiple sequence alignment software version 7: Improvements in performance and usability. *Molecular Biology and Evolution, 30*(4), 772–780. https://doi.org/10.1093/molbev/mst010

Kück, P., & Longo, G. C. (2014). FASconCAT-G: extensive functions for multiple sequence alignment preparations concerning phylogenetic studies. *Frontiers in Zoology, 11*(81). https://doi.org/10.1186/s12983-014-0081-x

Kück, P., & Meusemann, K. (2010). FASconCAT: Convenient handling of data matrices. *Molecular Phylogenetics and Evolution, 56*(3), 1115–1118. https://doi.org/10.1016/j.ympev.2010.04.024

Kumar, S., Stecher, G., & Tamura, K. (2016). MEGA7: Molecular evolutionary genetics analysis version 7.0 for bigger datasets. *Molecular Biology and Evolution, 33*(7), 1870–1874. https://doi.org/10.1093/molbev/msw054

Kvist, S. (2016). Does a global DNA barcoding gap exist in Annelida? *Mitochondrial DNA. Part a, DNA Mapping, Sequencing, and Analysis, 27*(3), 2241–2252. https://doi.org/10.3109/19401736.2014.984166

Langerhans, P. (1879). Die Wurmfauna von Madeira [Part I]. *Zeitschrift Für Wissenschaftliche Zoologie, 32*(4), 513–592.

Larsson, A. (2014). AliView: A fast and lightweight alignment viewer and editor for large datasets. *Bioinformatics, 30*(22), 3276–3278. https://doi.org/10.1093/bioinformatics/btu531

Lee, J. (1992). 한국산 영주갯지렁이 과(한형동물 문, 다모 강)의 계통분류학적 연구 [Doctoral dissertation, Ewha Womans University]. Ewha Research Repository. https://dspace.ewha.ac.kr/handle/2015.oak/194291

Lobo, J., Teixeira, M. A. L., Borges, L. M. S., Ferreira, M. S. G., Hollatz, C., Gomes, P. T., Sousa, R., Ravara, A., Costa, M. H., & Costa, F. O. (2016). Starting a DNA barcode reference library for shallow water polychaetes from the southern European Atlantic coast. *Molecular Ecology Resources, 16*(1), 298–313. https://doi.org/10.1111/1755-0998.12441

Madeira, F., Park, Y., & mi, Lee, J., Buso, N., Gur, T., Madhusoodanan, N., Basutkar, P., Tivey, A. R. N., Potter, S. C., Finn, R. D., & Lopez, R. (2019). The EMBL-EBI search and sequence analysis tools APIs in 2019. *Nucleic Acids Research, 47*(W1), W636–W641. https://doi.org/10.1093/nar/gkz268

Malmgren, A. J. (1867). *Annulata Polychaeta Spetsbergiæ, Grænlandiæ, Islandiæ et Scandinaviæ. Hactenus Cognita*. Ex Officina Frenckelliana.

Martin, D., Aguado, M. T., & Britayev, T. A. (2009). Review of the symbiotic genus *Haplosyllides* (Polychaeta: Syllidae), with a description of a new species. *Zoological Science, 26*(9), 646–655. https://doi.org/10.2108/zsj.26.646

Martin, D., & Britayev, T. A. (1998). Symbiotic polychaetes: Review of known species. *Oceanography and Marine Biology: An Annual Review, 36*, 217–340. https://doi.org/10.1201/b12646

Martin, D., & Britayev, T. A. (2018). Symbiotic polychaetes revisited: An update of the known species and relationships (1998–2017). *Oceanography and Marine Biology: An Annual Review, 56*, 371–448. https://doi.org/10.1201/9780429454455

Martin, D., Britayev, T. A., San Martín, G., & Gil, J. (2003). Inter-population variability and character description in the sponge-associated *Haplosyllis spongicola* complex (Polychaeta: Syllidae). *Hydrobiologia, 496*, 145–162. https://doi.org/10.1023/A:1026184529208

McIntosh, W. C. (1879). On a remarkably branched *Syllis* dredged by H.M.S. Challenger. *Journal of the Linnean Society London, 14*, 720–724. https://doi.org/10.1111/j.1096-3642.1879.tb02356.x

McIntosh, W. C. (1885). Report on the Annelida Polychaeta collected by H.M.S. Challenger during the years 1873–1876. *Challenger Reports, 12*, 189–208. https://doi.org/10.5962/bhl.title.6513

Meyer, M., & Kircher, M. (2010). Illumina sequencing library preparation for highly multiplexed target capture and sequencing. *Cold Spring Harbor Protocols, 5*(6). https://doi.org/10.1101/pdb.prot5448

Miglietta, M. P., Hourdez, S., Cowart, D. A., Schaeffer, S. W., & Fisher, C. (2010). Species boundaries of Gulf of Mexico vestimentiferans (Polychaeta, Siboglinidae) inferred from mitochondrial genes. *Deep-Sea Research Part II: Topical Studies in Oceanography, 57*(21–23), 1916–1925. https://doi.org/10.1016/j.dsr2.2010.05.007

Nguyen, L. T., Schmidt, H. A., Von Haeseler, A., & Minh, B. Q. (2015). IQ-TREE: A fast and effective stochastic algorithm for estimating maximum-likelihood phylogenies. *Molecular Biology and Evolution, 32*(1), 268–274. https://doi.org/10.1093/molbev/msu300

Nygren, A., Parapar, J., Pons, J., Meißner, K., Bakken, T., Kongsrud, J. A., Oug, E., Gaeva, D., Sikorski, A., Johansen, R. A., Hutchings, P. A., Lavesque, N., & Capa, M. (2018). A mega-cryptic species complex hidden among one of the most common annelids in the north east Atlantic. *PLoS ONE, 13*(6), e0198356. https://doi.org/10.1371/journal.pone.0198356

Oka, A. (1895). Über die Knospungsweise bei *Syllis ramosa*. *Zoologischer Anzeiger, 18*, 462–464.

Okada, Y. K. (1933). Two interesting syllids, with remarks on their asexual reproduction. *Mem. College of Sci., Kyoto Imperial University. Ser. B., 8*(3), 325–338.

Okada, Y. K. (1937). La stolonisation et les caracteres sexuels du stolon chez les syllidiens polychetes (Études sur les syllidiens III). *Japanese Journal of Zoology, 7*, 441–490.

Peng, Y., Leung, H. C. M., Yiu, S. M., & Chin, F. Y. L. (2012). IDBA-UD: A de novo assembler for single-cell and metagenomic sequencing data with highly uneven depth. *Bioinformatics, 28*(11), 1420–1428. https://doi.org/10.1093/bioinformatics/bts174

Perna, N. T., & Kocher, T. D. (1995). Patterns of nueleotide composition at fourfold degenerate sites of animal mitochondrial genomes. *Jounral of Molecular Evolution, 41*, 353–358. https://doi.org/10.1007/BF00186547

Ponz-Segrelles, G., Bleidorn, C., & Aguado, M. T. (2018). Expression of *vasa*, *piwi*, and *nanos* during gametogenesis in *Typosyllis antoni* (Annelida, Syllidae). *Evolution & Development, 20*, 132–145. https://doi.org/10.1111/ede.12263

Ponz-Segrelles, G., Glasby, C. J., Helm, C., Beckers, P., Hammel, J. U., Ribeiro, R. P., & Aguado, M. T. (2021). Integrative anatomical study of the branched annelid *Ramisyllis multicaudata* (Annelida, Syllidae). *Journal of Morphology, 282*(6), 900–916. https://doi.org/10.1002/jmor.21356

Prjibelski, A., Antipov, D., Meleshko, D., Lapidus, A., & Korobeynikov, A. (2020). Using SPAdes De Novo Assembler. *Current Protocols in Bioinformatics, 70*(1), e102. https://doi.org/10.1002/cpbi.102

Radashevsky, V. I., Pankova, V. V., Neretina, T. V., Stupnikova, A. N., & Tzetlin, A. B. (2016). Molecular analysis of the *Pygospio elegans* group of species (Annelida: Spionidae). *Zootaxa, 4083*(2), 239–250. https://doi.org/10.11646/zootaxa.4083.2.4

Read, G. (2001). Unique branching worm found in New Zealand. *Biodiversity Update (NIWA), 4*, 1 (only).

Renaud, G., Kircher, M., Stenzel, U., & Kelso, J. (2013). freeIbis: An efficient basecaller with calibrated quality scores for Illumina sequencers. *Bioinformatics, 29*(9), 1208–1209. https://doi.org/10.1093/bioinformatics/btt117

Renaud, G., Stenzel, U., & Kelso, J. (2014). LeeHom: Adaptor trimming and merging for Illumina sequencing reads. *Nucleic Acids Research, 42*(18), e141. https://doi.org/10.1093/nar/gku699

Ribeiro, R. P., Ponz-Segrelles, G., Helm, C., Egger, B., Bleidorn, C., & Aguado, M. T. (2020). A new species of *Syllis* including transcriptomic data and an updated phylogeny of Syllinae (Annelida: Syllidae). *Marine Biodiversity, 50*(31), 16. https://doi.org/10.1007/s12526-020-01046-y

San Martín, G., & Aguado, M. T. (2014). Family Syllidae. In A. Schmidt-Rhaesa (Ed.), *Handbook of Zoology. Annelida: Polychaetes* (pp. 1–68). De Gruyter.

Schroeder, P. C., Aguado, M. T., Malpartida, A., & Glasby, C. J. (2017). New observations on reproduction in the branching polychaetes, *Ramisyllis multicaudata* and *Syllis ramosa* (Annelida: Syllidae: Syllinae). *Journal of the Marine Biological Association of the United Kingdom, 97*(5), 1167–1175. https://doi.org/10.1017/S002531541700039X

Simon, C., Frati, F., Beckenbach, A., Crespi, B., Liu, H., & Flook, P. (1994). Evolution, weighting, and phylogenetic utility of mitochondrial gene sequences and a compilation of conserved polymerase chain reaction primers. *Annals of the Entomological Society of America, 87*(6), 651–701. https://doi.org/10.1093/aesa/87.6.651

Taboada, S., Serra Silva, A., Díez-Vives, C., Neal, L., Cristobo, J., Ríos, P., Hestetun, J. T., Clark, B., Rossi, M. E., Junoy, J., Navarro, J., & Riesgo, A. (2021). Sleeping with the enemy: Unravelling the symbiotic relationships between the scale worm *Neopolynoe chondrocladiae* (Annelida: Polynoidae) and its carnivorous sponge hosts. *Zoological Journal of the Linnean Society, 193*(1), 295–318. https://doi.org/10.1093/zoolinnean/zlaa146

Tang, C. Q., Leasi, F., Obertegger, U., Kieneke, A., Barraclough, T. G., & Fontaneto, D. (2012). The widely used small subunit 18S rDNA molecule greatly underestimates true diversity in biodiversity surveys of the meiofauna. *Proceedings of the National Academy of Sciences of the United States of America, 109*(40), 16208–16212. https://doi.org/10.1073/pnas.1209160109

Turon, M., Uriz, M. J., & Martin, D. (2019). Multipartner symbiosis across biological domains: Looking at the eukaryotic associations from a microbial perspective. *Msystems, 4*(4), 1–14. https://doi.org/10.1128/msystems.00148-19

Vivien, R., Wyler, S., Lafont, M., & Pawlowski, J. (2015). Molecular barcoding of aquatic oligochaetes: Implications for biomonitoring. *PLoS ONE, 10*(4), e0125485. https://doi.org/10.1371/journal.pone.0125485

Xia, X. (2018). DAMBE7: New and improved tools for data analysis in molecular biology and evolution. *Molecular Biology and Evolution, 35*(6), 1550–1552. https://doi.org/10.1093/molbev/msy073

Zattara, E. E., & Weisblat, D. A. (2020). Cellular and molecular mechanisms of segmentation in Annelida: An open question. In A. D. Chipman (Ed.), *Cellular processes in segmentation* (pp. 71–97). Taylor & Francis.

Zhang, Z., Schwartz, S., Wagner, L., & Miller, W. (2000). A greedy algorithm for aligning DNA sequences. *Journal of Computational Biology, 7*(1–2), 203–214. https://doi.org/10.1089/10665270050081478

Publisher's Note Springer Nature remains neutral with regard to jurisdictional claims in published maps and institutional affiliations.